


---

This is the **accepted version** of the journal article:

Raventos-Izard, Georgina; Potau, Josep Maria; Casado, Aroa; [et al.]. «The morphofunctional implications of the glenoid labrum of the glenohumeral joint in hominoids». *American Journal of Biological Anthropology*, Vol. 181, issue 2 (June 2023), p. 195-205. DOI 10.1002/ajpa.24729

---

This version is available at <https://ddd.uab.cat/record/283627>

under the terms of the  **CC BY** COPYRIGHT license

1 **The morphofunctional implications of glenoid *labrum* of the glenohumeral joint in**  
2 **hominoids**

3 Georgina Raventós-Izard<sup>1\*</sup>, Josep M<sup>a</sup> Potau<sup>2,3</sup>, Aroa Casado<sup>2,3</sup>, Juan F Pastor<sup>4</sup>, Julia  
4 Arias-Martorell<sup>1,5\*</sup>

5 1 Institut Català de Paleontologia Miquel Crusafont, Universitat Autònoma de  
6 Barcelona, Edifici ICTA-ICP, c/ Columnes s/n, Campus de la UAB, 08193 Cerdanyola  
7 del Vallès, Barcelona, Spain.

8 2 Unit of Human Anatomy and Embryology, Faculty of Medicine, University of  
9 Barcelona, c/Casanova 143 08036, Barcelona, Spain.

10 3 Institut d'Arqueologia de la Universitat de Barcelona (IAUB), Faculty of Geography  
11 and History, University of Barcelona, 08001 Barcelona, Spain.

12 4 Museo Anatómico, Departamento de Anatomía y Radiología, Facultad de Medicina,  
13 Universidad de Valladolid, c/Ramón y Cajal 7, 47005, Valladolid, Spain.

14 5 School of Anthropology and Conservation, Marlowe Building, University of Kent,  
15 Canterbury, CT2 7NR, UK

16

17 \*corresponding author

18 *Email address:* georgina.raventos@icp.cat (G. Raventós-Izard) | julia.arias@icp.cat (J.  
19 Arias-Martorell)

20

21 **Abstract**

22 **Objectives.** A morphocline of the glenoid cavity has been used to infer  
23 differences in locomotor behaviors; however, the glenoid cavity is surrounded by  
24 the glenoid *labrum*, a fibrocartilaginous structure that could influence the  
25 functionality of the glenoid. The objectives of this study are to explore the effects

26 of the glenoid *labrum* on the area, depth, and morphology of the glenoid cavity in  
27 primates.

28 **Material and Methods.** Photogrammetry was used to build 3D models of  
29 the glenoid, with and without the *labrum*, and three- (3D) and two-dimensional  
30 (2D) geometric morphometrics (GM) was applied. 2D areas were collected from  
31 zenithal images for glenoids with and without *labrum* to evaluate the availability of  
32 articular surface area.

33 **Results.** In the 2D GM the morphocline is present in the dry-bone sample  
34 but not with the presence of the glenoid *labrum*. In the 3D GM there are differences  
35 between species mainly concerning the depth of the glenoid cavity. 2D areas reveal  
36 that the amount of articular area of the glenoid cavity increases with the presence of  
37 the *labrum*, particularly in humans.

38 **Discussion.** The glenoid *labrum* changes the shape, increases the depth and  
39 the surface area of the glenoid cavity, particularly in humans. Therefore, the  
40 glenoid *labrum* might hold a functional role, increasing the stability of the  
41 glenohumeral joint of primates in general, and especially in humans.

42

43 **Keywords**

44 Geometric morphometrics; Photogrammetry; Shoulder joint; Glenoid cavity; Apes

45       **1. Introduction**

46       The morphology of the glenohumeral (shoulder) joint reflects the locomotor  
47 and postural behavior of different taxa (Jungers, 1991); in this regard, in primates,  
48 and in particular, in apes, the glenohumeral joint has been widely used to explore  
49 the differences in locomotor behaviors (e.g., Corruccini & Ciochon, 1978; Larson  
50 & Stern, 1986; Larson, 1988; Larson, 1995; MaClatchy, Gebo, Kityo, & Pilbeam,  
51 2000; Roberts, 1974).

52       The glenohumeral joint of apes—including gibbons and siamangs (hylobatids)  
53 and great apes (gorillas (*Gorilla*), chimpanzees (*Pan*), orangutans (*Pongo*), and  
54 humans (*Homo*))—has anatomical features that enable the forelimbs to be held in  
55 overhead positions that are required in locomotor activities such as suspension or  
56 vertical climbing (Ashton & Oxnard, 1964; Larson, 1988; Larson, 1995;  
57 MaClatchy et al., 2000; Roberts, 1974). These features include a cranially-oriented  
58 glenoid fossa (Ashton & Oxnard, 1964), a lateral projection of the glenohumeral  
59 joint (Ashton & Oxnard, 1964), and a small, oval, and flat articular surface of the  
60 glenoid cavity articulating with a large humeral head (Ashton & Oxnard, 1964;  
61 Fleagle, 2013; Godfrey, Sutherland, Boy, & Gomberg, 1991; Larson, 1988; Larson,  
62 1995). The size difference in hominoids between the small glenoid fossa and the  
63 large articular surface of the humeral head is indicative of increased mobility of the  
64 glenohumeral joint in hominoids (Larson & Stern, 1986; Larson, 1988; Larson,  
65 1993; Larson, 1995; Roberts, 1974; Rose, 1989). Furthermore, an oval glenoid  
66 cavity, which is found in hominoids, some atelines, and cursorial mammals,  
67 presents a broader dorsoventral width relative to craniocaudal length, and a  
68 moderate craniocaudal and dorsoventral curvatures, allowing a wide range of axial  
69 movements (MaClatchy et al., 2000; Roberts, 1974).

70 A kinematic study by Chan (2007) suggested that hominoids have less  
71 glenohumeral mobility than monkeys. Subsequent studies by the same author on  
72 shoulder mobility (Chan, 2008) have shown that a dorsally-positioned scapula may  
73 enhance pectoral girdle movement in hominoids thus making their overall arm  
74 mobility not different from monkeys—except for hylobatids which possess the  
75 highest shoulder mobility among all primates included in the study. However, no  
76 gorilla or orangutan specimens were included in the studies (Chan, 2007, 2008),  
77 therefore differences in shoulder range of motion between African and Asian apes  
78 were not taken into account (Isler, 2005). Humans, which were the best hominoid  
79 species represented in the study (Chan, 2007), have particular adaptations to  
80 forelimb manipulation behaviors, which may have an effect on the findings,  
81 especially regarding the overall glenohumeral mobility range in hominoids.

82 Nonhominoid primates (e.g., cercopithecoids), have a more proportionate  
83 glenoid cavity relative to the humeral head, with a larger contact area between the  
84 two structures, which limits the range of movement but favors a more stable  
85 glenohumeral joint (Larson, 1995; Rose, 1989). In addition, nonhominoid primates  
86 have a lock mechanism when the humerus is fully abducted, suggesting that the  
87 humerus is not mobile in maximally protracted position due to the blocking of a  
88 cranially-located lip of the glenoid fossa into the bicipital groove when the humerus  
89 is fully abducted (Chan, 2007). Hominoids do not exhibit a lock mechanism  
90 because their distally-situated greater tubercle makes it impossible for the non-  
91 projecting superior lip of the glenoid fossa to lock into the bicipital groove (Chan,  
92 2007); this may be an adaptation to overhead positions of the forelimbs.

93 Glenoid depth depends on the morphological configuration of the fossa: oval  
94 glenoid cavities are flat craniocaudally and dorsoventrally; pear-shaped glenoids

95 have a marked craniocaudal curvature (MaClatchy et al., 2000; Roberts, 1974), due  
96 to the presence of the superior lip. This feature may affect its contact area with the  
97 humeral head, thus flatter glenoid cavities may be indicative of a more mobile but  
98 less stable glenohumeral joint, and vice versa (Arias-Martorell, 2019). In turn, the  
99 craniocaudal curvature in pear-shaped glenoids would favor flexion/extension over  
100 axial movements (MaClatchy et al., 2000; Roberts, 1974).

101 No morphological features of the glenoid cavity seem to be related to sex,  
102 activity, or laterality in humans (Macias & Churchill, 2015). However, kinematics  
103 studies show that the frequency of overhead positions of the forelimbs and the  
104 range of motion of the shoulder is higher in juvenile and female hominoids, mainly  
105 due to body size (Isler, 2005). Moreover, some primate species display high degree  
106 of lateralization (i.e., handedness) (Hopkins et al., 2004; Margiotoudi et al., 2019;  
107 Morino et al., 2017). However, there is no study testing intraspecific  
108 morphological differences of the glenoid cavity in nonhuman primates therefore  
109 the influence of sex, age, and laterality in the glenoid cavity morphology it is not  
110 known.

111 *In vivo*, the glenoid cavity presents an additional soft-tissue structure, the  
112 glenoid *labrum* (or rim), which surrounds it in its entirety. The glenoid *labrum* is a  
113 fibrocartilaginous structure, which, due to its location on the margins of the glenoid  
114 cavity, may expand the articular surface area of the glenoid cavity, thus enabling a  
115 better contact between the glenoid and the humeral head (Arias-Martorell, 2019;  
116 Howell & Galinat, 1989). It may also affect the depth of the glenoid, making it  
117 more concave (Howell & Galinat, 1989). Despite its impact in glenoid morphology,  
118 the function of the glenoid *labrum* has been not studied in detail in nonhuman  
119 primates (Arias-Martorell, 2019).

120 While several studies have explored the three-dimensional morphology of the  
121 dry-bone glenoid (e.g., Arias-Martorell et al., 2015; Macias & Churchill, 2015;  
122 Young, 2008), to the best of our knowledge, the morphology of the *labrum* has not  
123 been quantified in non-human primates to date. In humans, in the clinical literature,  
124 the morphology and role of the *labrum* has been studied using Magnetic Resonance  
125 Imaging (MRI) scans (e.g., Beltran, et al., 1997). We used photogrammetry to  
126 record the 3D morphology of soft tissue (i.e., the glenoid *labrum*) since it has been  
127 widely used in the anthropological field for documentation, tool reconstruction, and  
128 skeletal modeling (e.g., Katz & Friess, 2014), even though it has never been used to  
129 record cartilage tissue.

130 This study explores the effects of the glenoid *labrum* regarding the function and  
131 morphology of the glenoid cavity and the glenohumeral joint. We examine how the  
132 glenoid *labrum* influences the area, depth, and shape of the glenoid cavity in  
133 primates to determine whether its presence affects the functionality of the  
134 glenohumeral joint. Additionally, this study will examine the utility of  
135 photogrammetry as a soft tissue reconstruction technique.

136

## 137 **2. Material and Methods**

### 138 2.1. Sample

139 Our sample consisted of frozen, non-chemically preserved cadavers of 22  
140 primates (Table 1 and SI Table 1), comprising: humans (*Homo sapiens*, N=4),  
141 chimpanzees (*Pan troglodytes*, N=6), gibbons (*Hylobates lar*, N=1, and *Nomascus*  
142 *gabriellae*, N=1), siamangs (*Symphalangus syndactylus*, N=1), and cercopithecines  
143 (*Chlorocebus aethiops*, N=1, *Cercocebus atys lunulatus*, N=1, *Cercopithecus*  
144 *ascanius*, N=1, *Miopithecus ogouensis*, N=1, *Macaca silenus*, N=1, *Macaca*

145 *sylvanus*, N=1, *Macaca tonkeana*, N=1, *Papio hamadryas*, N=2). We obtained the  
146 human sample from the Body Donation Service of the Faculty of Medicine of the  
147 University of Barcelona (Barcelona, Spain). We obtained the non-human primate  
148 sample from the Anatomical Museum of the University of Valladolid (Valladolid,  
149 Spain), which centralizes the processing of deceased primates from zoos and  
150 animal rescue centers from Spain. All individuals included in the study died from  
151 external causes independent of this study.

152 We performed dissections of the cadavers, which followed the  
153 recommendations and ethical guidelines of the University of Barcelona and the  
154 Body Donation Service. We removed all the muscles and soft tissue surrounding  
155 the glenohumeral joint, of which we carefully removed the capsule and separated  
156 the two components (the humeral head and the glenoid cavity of the scapula) as  
157 well, to expose the glenoid *labrum*. We then recorded the cartilaginous structure  
158 surrounding the glenoid cavity by taking a cloud of photographs (photogrammetry)  
159 of the scapula, with each picture taken from a slightly different angle and position  
160 (see below). The same procedure was followed for glenoid cavities without the  
161 *labrum* after removing the remaining soft tissue.

## 162 2.2. Photogrammetry

163 We took the pictures with a Canon EOS 1000D camera with 10 megapixels and  
164 a 18-15 mm lens, in automatic mode or close-up. Good overlap between pictures  
165 was obtained by moving the camera only a few centimeters between shots. The  
166 clouds or sets of pictures taken ranged in number from 17 to 101 per set. These  
167 were imported into Agisoft Metashape 1.7.3 (St. Petersburg, Russia) without any  
168 prior treatment. For building the 3D models, we generated a sparse point cloud,  
169 which we used to create 3D meshes. We were able to obtain 3D models for a subset



170 of the sample only, comprising *Homo sapiens* (N=4), *Pan troglodytes* (N=4),  
171 *Hylobates lar* (N=1), *Nomascus gabriellae* (N=1), *Chlorocebus aethiops* (N=1),  
172 *Cercocebus atys lunulatus* (N=1), *Cercopithecus ascanius* (N=1), *Miopithecus*  
173 *ogouensis* (N=1), and *Papio hamadryas* (N=2) (SI Table 2).

### 174 2.3. Geometric morphometrics

175 Three-dimensional geometric morphometrics were used to explore the shape of  
176 the glenoid cavity with and without *labrum* using the 3D models obtained via  
177 photogrammetric reconstruction (N=16). For the complete sample (N=22), we  
178 performed two-dimensional geometric morphometrics using the zenithal image of  
179 each glenoid cavity with and without *labrum* extracted from the cloud of  
180 photographs obtained for photogrammetric reconstruction.

181 We applied two landmark protocols (SI Table 3 and Fig. 1): a protocol of six  
182 landmarks (Fig. 1A, 1C) to the 3D sample, with and without *labrum*, using  
183 Landmark Editor v. 3.0 (Wiley et al., 2005) and a protocol of eight landmarks (Fig.  
184 1B, 1D) to the zenithal images (from the photogrammetry sets) of the glenoid  
185 cavity, with and without *labrum*, using tpsDig2 v. 2.31.8 (Rohlf, 2015). Both  
186 landmark protocols capture the glenoid cavity morphology, however, the former  
187 contemplates depth, which is a feature that can only be explored with 3D data,  
188 whereas the later puts emphasis on the contour, which is more easily recorded with  
189 2D data.

190 Using the ‘Morpho’ v. 2.8 package (Schlager, 2017) in R v. 4.1.1 (R Core  
191 Team, 2021) we applied a General Procrustes Analysis (GPA) to rotate, scale (to  
192 size 1 of the centroid), and translate all shapes in each sample subset (3D, with and  
193 without *labrum*, and 2D, with and without *labrum*). We carried out a Principal  
194 Component Analyses (PCA) for each sample subset with the GPA coordinates to

195 identify shape variation between groups (cercopithecoids, chimpanzees, hylobatids,  
196 and humans). In addition, a phylogenetically-adjusted PCA (phy-PCA) was  
197 conducted to explore the shape changes and group distribution accounting for the  
198 phylogenetic structure underlying our data (Adams et al., 2020) for each sample  
199 subset. We downloaded a molecular-based time-calibrated phylogenetic tree from  
200 10kTrees website v. 3 (Arnold, Matthewa, & Nunn, 2010), which we used for both  
201 the phy-PCA and PGLS analyses (below).

202 Ordinary least-squares (OLS) regression of PC scores (PC1 and PC2) vs. log-  
203 transformed centroid size (ln CS), and phylogenetic generalized least-squares  
204 (PGLS; Adams, 2014) of species mean coordinates against the mean centroid size  
205 of each group were computed to evaluate allometry using the ‘geomorph’ v. 3.1.1 R  
206 package (Adams et al., 2020) in each sample subset.. All plots were done using the  
207 packages ‘ggpubr’ v. 0.4.0. and ‘ggplot2’ v. 3.3.6.

208 Morphological differences regarding the present/absence of the glenoid *labrum*  
209 were tested by performing a Procrustes ANOVA on the 2D and the 3D sample with  
210 Bonferroni post-hoc test, using the ‘geomorph’ v. 3.1.1 R package (Adams et al.,  
211 2020).

#### 212 2.4. 2D areas

213 From the zenithal images, we calculated two-dimensional areas (with and  
214 without glenoid *labrum*) with ImageJ 1.53e (Schneider, Rasband, & Eliceiri,  
215 2012) and we visualized the group differences through a box-and-whisker plot.

216

### 217 **3. Results**

#### 218 3.1. Geometric morphometrics

##### 219 *Principal Components Analyses*

220       **3D geometric morphometrics PCAs.** The PCA for the glenoid without *labrum*  
221 yields 11 principal components (PCs), of which the first six components explain  
222 89.9% of the total variance (Fig. 2A, SI Fig. 1, 2, 3, 4, and Table 2). We did not  
223 consider PCs with <5% variance throughout the analyses as they did not yield any  
224 meaningful patterns, but all are reported in Table 2. PC1 is driven by differences in  
225 glenoid depth, with individuals with more negative scores having deeper glenoids.  
226 Group differences are not clearly established, but are somewhat clearer in PC1,  
227 especially for hylobatids, which occupy a different space from the other groups,  
228 and *Homo sapiens*, which cluster together in the middle of the scatterplot.

229       The PCA for the glenoid with *labrum* yields 11 PCs, of which the first six  
230 components explain 92.1 % of the total variance (Fig. 2B, SI Fig. 5, 6, 7, 8, and  
231 Table 2). PC1 shows differences between *Pan* and *Homo*, yet cercopithecoids  
232 overlap with every group (with hylobatids and chimpanzees to a lesser extent). PC1  
233 mainly represents depth variation, whereas PC2 variation is driven by glenoid  
234 outline differences, where, in the positive end, scores represent a glenoid with an  
235 elongated mid-inferior portion, and, in the negative end, they represent glenoids  
236 with an extended mid-superior portion.

237       **2D geometric morphometrics PCAs.** The PCA for the glenoid without *labrum*  
238 yields 12 PCs, of which the first three components explain 83.8 % of the total  
239 variance (Fig. 3A, SI Fig. 9, and Table 2). PC1 represent variation between pear-  
240 shaped and oval glenoids, in both cases with elongated shape in contrast with PC2,  
241 which shows differences between elongated and rounded glenoids, and display a  
242 better group separation, although cercopithecoids and *Pan* overlap with the other  
243 groups.

244       The PCA for the glenoid with *labrum* yields 12 PCs, of which the first five

245 components explain 85.2% of the total variance (Fig. 3B, SI Fig. 10, 11, 12, and  
246 Table 2). PC1 shows differences between rounded and pear-shaped glenoids,  
247 whereas PC2 shows slight differences in elongation.

#### 248 *Phylogenetic Principal Components Analyses*

249 **3D geometric morphometrics phy-PCAs.** The phy-PCA for the glenoid  
250 without *labrum* yields eight PCs, of which the first four components explain 91.8%  
251 of the total variance (Fig. 4A and Table 3). Hominoids cluster together in the  
252 middle of the scatterplot, however the cercopithecoids variability is widest and they  
253 overlap with every other group. Shape changes are driven by depth in both PC1 and  
254 PC2, although less markedly than in the non-phylogenetically adjusted PCA.

255 The phy-PCA for the glenoid with *labrum* yield eight PCs, of which the first  
256 five components explain 94.2 % of the total variance (Fig. 4B and Table 3).  
257 *Nomascus* is separated from the other groups, and while PC2 shows differences  
258 between *Pan* and *Homo*, cercopithecoids overlap with every group. PC1 shows  
259 differences in depth and PC2 shows differences in glenoid outline, with somewhat  
260 rounder glenoids on the negative end, and glenoids with an elongated mid-superior  
261 portion on the negative end.

262 **2D geometric morphometrics phy-PCAs.** The phy-PCA for the glenoid  
263 without *labrum* yield 12 PCs, of which the first four components explain 93.0 % of  
264 the total variance (Fig. 5A and Table 3). Hylobatids fall outside the variability of  
265 cercopithecoids, which encompass that of the other hominoids, however, every  
266 hylobatid species occupies a different location in the morphospace, not clustering  
267 together. PC1 represent variation between pear-shaped and oval glenoids and PC2  
268 differences between elongated and rounded glenoids.

269 The PCA for the glenoid with *labrum* yields 12 PCs, of which the first five

270 components explain 92.7% of the total variance (Fig. 5B and Table 3). Both PCs  
271 represent variation between pear-shaped (positive end) and oval (negative end)  
272 glenoids.

### 273 *OLS and PGLS regressions*

274 No PC is significantly correlated with ln CS (for all sample subsets,  $p > 0.05$ ;  
275 Table 4), meaning size does not account for shape variation. The PGLS on mean  
276 group coordinates and mean centroid size is not significant ( $p > 0.05$  for all sample  
277 subsets; Table 4). Centroid size explain very little in all 2D subsets and 3D subset  
278 without *labrum* ( $R^2 < 0.10$ ), however, for the 3D subset, centroid size explained  
279 13% of the variance without *labrum* in 3D ( $R^2 = 0.134$ ) and 12% of the variance  
280 with *labrum* in 3D ( $R^2 = 0.121$ ; Table 4), but did not reach significance ( $p = 0.314$   
281 and  $p = 0.352$ , respectively).

### 282 *Procrustes ANOVA*

283 There is no significant difference between species, regardless of the presence of  
284 the *labrum*, in both 2D ( $Z = 0.469$ ;  $p = 0.320$ ) and 3D samples ( $Z = 0.194$ ;  $p =$   
285  $0.440$ ); however, within the Bonferroni post-hoc using 2D data, some intragroup  
286 differences between presence and absence of *labrum* were found for *Cercopithecus*  
287 *ascanius*, *Chlorocebus aethiops*, *Macaca sylvanus*, *Miopithecus ogouensis* for the  
288 cercopithecoids, and *Nomascus gabriellae* for hominoids (the full results of the  
289 Bonferroni post-hoc can be found the supplementary material SI Table 4, for the  
290 2D sample, and SI Table 5, for the 3D sample).

### 291 3.2. 2D areas

292 The box-and-whisker plot (Fig. 6) shows a trend to an increase in absolute  
293 values of glenoid cavity surface area with the presence of *labrum* in all groups, and  
294 that the increase is most acute in humans and, to a lesser degree, in chimpanzees.

295

#### 296 **4. Discussion**

297 We have investigated the effects of the glenoid *labrum* in relation to the  
298 function and morphology of the glenoid cavity and the overall glenohumeral joint.  
299 Overall, the results suggest that the presence of the glenoid *labrum* might change  
300 the depth, area, and shape of the contour of the glenoid cavity. We further discuss  
301 the results of the 3DGM analyses and surface area availability analyses below.

##### 302 4.1. Geometric morphometrics

303 Our results indicate that the morphology and variability of dry-bone glenoid  
304 cavities are comparable to that reported by previous works of hominoids (Arias-  
305 Martorell et al., 2015; Larson, 1998; Larson 2013; Macias & Churchill, 2015;  
306 Roberts, 1974). In most studies the skeletonized glenoid cavities of hominoids tend  
307 to display an intermediate morphology between oval and round, with hylobatids  
308 having the roundest glenoids. Cercopithecoids, on the other hand, are found here to  
309 display a great amount of variation, not showing the marked pear-shaped  
310 morphology reported in previous works (e.g., Arias-Martorell et al., 2015; Selby,  
311 Lovejoy, & Byron, 2020). This is the case of the two *Papio* and the *Cercocebus*  
312 individuals, which do not present a pear-shaped glenoid. Instead, they present a  
313 single notch on one side of the glenoid cavity, making the overall glenoid contour  
314 morphology more hominoid-like—and thus overlapping with apes.

315 When the *labrum* is present, the morphology of the glenoid cavity differs from  
316 its morphology observed in dry-bone material. In the 2D analyses, intragroup  
317 variation increases, and group distribution within the morphospace is not as clear-  
318 cut as without the presence of the glenoid *labrum* (e.g., Roberts, 1974). The glenoid  
319 cavity of chimpanzees without *labrum* displays an intermediate morphology; the

320 presence of the *labrum* changes the morphology of the glenoid to a more elongated  
321 structure, due to uneven thickness of the *labrum*, which appears to be thicker at the  
322 inferior margin. The resulting morphology of glenoid cavities of chimpanzees with  
323 *labrum* is closer to quadrupedal cercopithecoids than to arboreal apes, which could  
324 potentially be related to functional demands of the more terrestrial locomotor  
325 behavior of chimpanzees (e.g., knuckle-walking). Gorillas, which are in general  
326 less arboreal than chimpanzees in adulthood (Hunt, 1991), should be included in  
327 the analysis to test this hypothesis in future studies.

328 In general, the changes in thickness of the *labrum* appears to be particular to  
329 each species in the present study; in this regard, thickness varies along the glenoid  
330 cavity margin thus changing its morphology. Certainly, there are significant  
331 differences in the glenoid cavity morphology with and without *labrum* in four  
332 groups of cercopithecoids (*Chlorocebus aethiops*, *Cercopithecus ascanius*,  
333 *Miopithecus ogouensis*, and *Macaca sylvanus*) and one hominoid (*Nomascus*). The  
334 sample size of all our groups is very small, therefore, it is possible that larger  
335 samples might lead to more significant differences in thickness and morphology in  
336 future studies.

337 The 3D analyses allow the characterization of glenoid depth and show a clearer  
338 group separation than the 2D analyses. The presence of the *labrum* increases the  
339 depth of the glenoid and depth increase is the main feature distinguishing  
340 hominoids from cercopithecoids. Among hominoids, hylobatids show the most  
341 increase in depth. *Cercocebus* (which morphologically resembled hominoids in the  
342 2D analyses), when depth is considered, appears different from *Pan* and *Homo*.  
343 That is not the case for *Papio*, whose glenoid depth appears to be more hominoid-  
344 like (together with its glenoid contour morphology). Intriguingly, *Papio* is a

345 terrestrial quadruped, therefore, more studies are needed to evaluate whether there  
346 are similarities in *Papio* and hominoids regarding forearm use that might account  
347 for their resemblance in glenohumeral joint morphology.

348 In the case of humans, the glenoid *labrum* seems to be increasing the depth of  
349 the glenoid cavity. Dry-bone glenoid cavities of humans are already deeper than  
350 other apes in our study, but the presence of a thick and large *labrum* considerably  
351 contributes to the ball-and-socket nature of the human glenohumeral joint. The  
352 head of the humerus moves through the socket structure created by the glenoid  
353 cavity and the *labrum* in humans (Howell & Galinat, 1989), therefore, the depth  
354 increase afforded by the *labrum* in humans might be indicative of an improvement  
355 in the stability of the glenohumeral joint due to a better articular contact between  
356 the glenoid cavity and the humeral head. The manipulatory abilities of humans  
357 might demand more stability at the glenohumeral joint to aid in fine motor skills  
358 and arm repositioning capabilities for hand manipulation—as is the case of humeral  
359 torsion, which is related to hand manipulation (Larson, 2013), a greater stability of  
360 the glenohumeral joint could also represent additional manipulation-related features  
361 of the human arm (Larson, 2013). However, more studies are needed to further  
362 assess this possibility.

363 The phylogenetic relationships between the groups included in this study do not  
364 seem to influence the shape of the glenoid cavity with or without *labrum*, thus, the  
365 morphological characteristics of the glenoid found here are more probably related  
366 to function than to phylogeny. However, larger samples that would enable other,  
367 more accurate tests (such as phylogenetic signal analyses) have to be undertaken in  
368 the future to further evaluate the influence of phylogeny in glenoid shape with and  
369 without *labrum*.



370 4.2. Glenoid cavity surface area availability

371 The regression between shape and centroid size—a proxy for body mass—even  
372 when adjusted for phylogenetic relationships between groups, does not yield  
373 significant results. Therefore, body mass does not seem to be influencing the  
374 morphological changes in glenoid shape with or without *labrum* either in the 2D or  
375 3D subsets. However, the reported values of the 2D area, depicted in the box-and-  
376 whisker plot (which are absolute, not relative), show noticeable body mass  
377 differences between groups. As such, more analyses are needed to ascertain the  
378 influence of body mass regarding the thickness of the *labrum* in larger species.

379 Nevertheless, an overall intragroup increase in articular surface area in glenoid  
380 cavities with *labrum* in the 2D surface area values can be observed. Humans  
381 display the most acute increase in articular surface area of all groups, followed by  
382 chimpanzees. Even if related to differences in body mass, the intragroup increase in  
383 surface area does not preclude the possibility of a reduced size gap between glenoid  
384 cavity and the humeral head for all the species included in the analyses, but  
385 particularly so for humans when the *labrum* is present. This might influence the  
386 functionality of the glenohumeral joint and could potentially have an impact on the  
387 interpretations associated with joint surface availability derived from dry-bone  
388 material alone.

389 Finally, of particular interest are the functional inferences derived from fossil  
390 material where the characteristics of the *labrum* cannot be ascertained. For  
391 example, the Early Miocene ape *Morotopithecus* is considered to have engaged in  
392 suspensory behaviors based on the morphology of its glenoid cavity (MacLatchy et  
393 al., 2000). However, in light of the results found here, functional inferences derived  
394 from the morphology of dry-bone glenoid cavities might not reflect the

395 functionality of the glenohumeral joint *in vivo*. More studies are needed in order to  
396 better characterize the relationship between dry-bone glenoid cavity morphology  
397 and the *labrum*, and, in general, to better ascertain the influence of soft tissue in  
398 bone and joint function. In the same vein, more sample is needed to confirm the  
399 trends found in this study regarding changes in glenoid surface area and  
400 morphology.

#### 401 4.3. Limitations

402 Several limitations have been identified with our study which need to be  
403 addressed. The need to work with frozen fresh cadaveric samples to characterize  
404 soft tissue morphology is a significant limitation for this study because it severely  
405 limits the sample sizes we can accrue per each group due to availability of primates  
406 for dissection. This is also an issue for obtaining wide-ranging age and sex  
407 representation, and, especially, for acquiring data on both left and right sided  
408 glenoid cavities, which could be introducing a bias in species that show some  
409 degree of handedness. However, to the best of our knowledge, there are no studies  
410 exploring the effects of handedness on forelimb morphology and vice versa,  
411 therefore, more studies are needed to understand this potential bias introduced in  
412 our study. Another issue identified is the relative lack of locomotor diversity  
413 represented in the sample, particularly among cercopithecoids. Introducing groups  
414 such as colobines, for example, which show behaviors such as leaping and even  
415 suspension (Byron & Covert, 2004), or non-catarrhine monkeys such as atelids,  
416 which also show a diversity of locomotor behaviors, some of which convergently  
417 with apes (Cant, Youlatos & Rose, 2001) would be a priority in future studies.

418 In addition, we encountered some limitations with photogrammetry (for a  
419 review on the method and its use see, e.g., Fourie, Damstra, Gerrits, & Ren, 2011,

420 and references therein) when used to record soft tissue anatomy: good  
421 photogrammetric reconstructions did not depend on number of pictures taken, since  
422 we obtained good to medium quality 3D digital surface images with sets of pictures  
423 ranging from 17 to 101, as well as some low-quality reconstructions with 100-  
424 picture sets (e.g., a *Nomascua gabriellae* individual (NG03); SI Table 1). Other  
425 factors that influenced the quality of reconstructions were lighting conditions,  
426 keeping a continuous set of overlapping pictures in all axes, and maintaining focal  
427 distance, which was not always possible (oftentimes necropsy/dissection labs have  
428 limited conditions and space to properly set up equipment). The more homogenous  
429 bone tissue resulted in 3D digital surface images of good quality in all instances.

430

## 431 **5. Conclusions**

432 The glenoid cavity shape changes depending on whether the *labrum* is present,  
433 thus some functional inferences (e.g., high mobility in humans) of the glenoid  
434 would not be consistent with the functional interpretations of glenoid cavities with  
435 the presence of *labrum*. The presence of the glenoid *labrum* increases the depth and  
436 area of the glenoid cavity, extending contact with the head of the humerus, thus  
437 suggesting that the stability of the glenohumeral joint is improved and its mobility  
438 might be more limited than previously anticipated, particularly in humans.

439

## 440 **Acknowledgements**

441 We are grateful to A. Urciuoli for their help with the analyses. This work is part of  
442 R+D+I project PID2020-116908GB-I00, funded by the *Agencia Estatal de*  
443 *Investigación* of the Spanish Ministry of Science and Innovation  
444 (MCIN/AEI/10.13039/501100011033/). It is also funded by MCIN and the European

445 Union (FSE+) through *Ayudas para Contratos Predoctorales para la Formación de*  
446 *Doctores* (FPI) of the Agencia Estatal de Investigación; the Generalitat de Catalunya  
447 (AGAUR BP-H2020 MSCA-Cofund No. 801370 to JAM), the Spanish Ministry of  
448 Economy and Competitivity of Spain (MINECO) and the EU (FEDER) (CGL2014-  
449 52611-C2-2-P to JMP), and the University of Barcelona (APIF-UB 2016/2017 to AC).

450

#### 451 **Data availability statement**

452 The data that support the findings of this study are openly available in Zenodo  
453 (Zenodo.org) at <http://doi.org/10.5281/zenodo.7569015>.

454

#### 455 **References**

456

457 Adams, D., Collyer, M., Kaliontzopoulou, A., & Sherratt, E. (2020). Geomorph:  
458 geometric morphometric analyses of 2D/3D landmark data. R package  
459 version 3.2, 1.

460 Arias-Martorell, J. (2019). The morphology and evolutionary history of the  
461 glenohumeral joint of hominoids: A review. *Ecology and Evolution*, 9, 703-  
462 722. <https://doi.org/10.1002/ece3.4392>

463 Arias-Martorell, J., Potau, J. M., Bello-Hellegouarch, G., & Pérez-Pérez, A.  
464 (2015a). Like Father, Like Son: Assessment of the Morphological Affinities  
465 of A.L. 288–1 (*A. afarensis*), Sts 7 (*A. africanus*) and Omo 119–73–2718  
466 (*Australopithecus sp.*) through a three-dimensional shape analysis of the  
467 shoulder joint. *PLoS ONE*, 10, e0117408.

468 Arnold, C., Matthews, L. J., & Nunn, C. L. (2010). The 10kTrees website: a new  
469 online resource for primate phylogeny. *Evolutionary Anthropology*, 19, 114-

470 118. <https://doi.org/10.1002/evan.20251>

471 Ashton, E. H., & Oxnard, C. E. (1964). Functional adaptations in the primate  
472 shoulder girdle. *Proceedings of the Zoological Society of London*, 142, 49-  
473 66. <https://doi.org/10.1111/j.1469-7998.1964.tb05153.x>

474 Beltran, J., Rosenberg, Z. S., Chandnani, V. P., Cuomo, F., Beltran, S., & Rokito,  
475 A. (1997). Glenohumeral instability: evaluation with MR arthrography.  
476 *RadioGraphics*, 17, 657-673.  
477 <https://doi.org/10.1148/radiographics.17.3.9153704>

478 Byron, C. D. & Covert, H. H. (2004). Unexpected locomotor behaviour:  
479 brachiation by an Old World monkey (*Pygathrix nemaeus*) from Vietnam.  
480 *Journal of Zoology*, 263, 101-106. <https://doi:10.1017/S0952836904004935>

481 Cant, J. G., Youlatos, D., & Rose, M. D. (2001). Locomotor behavior of *Lagothrix*  
482 *lagothericha* and *Ateles belzebuth* in Yasuni National Park, Equador: general  
483 patterns and nonsuspensory modes. *Journal of Human Evolution*, 41, 141-  
484 166. <https://doi.org/10.1006/jhev.2001.0485>

485 Chan, L. K. (2007). Glenohumeral mobility in primates. *Folia Primatologica*, 78,  
486 1-18. <https://doi.org/10.1159/000095682>

487 Chan, L. K. (2008). The range of passive arm circumduction in primates: do  
488 hominoids really have more mobile shoulders? *American Journal of*  
489 *Physical Anthropology*, 136, 265-277. <https://doi.org/10.1002/ajpa.20800>

490 Corruccini, R. S., & Ciochon, R. L. (1978). Morphocline variation in the  
491 anthropoid shoulder. *American Journal of Physical Anthropology*, 48, 539-  
492 542. <https://doi.org/10.1002/ajpa.1330480415>

493 Fourie, Z., Damstra, J., Gerrits, P. O., & Ren, Y. (2011). Evaluation of  
494 anthropometric accuracy and reliability using different three-dimensional

495 scanning systems. *Forensic science international*, 207, 127-134.  
496 <https://doi.org/10.1016/j.forsciint.2010.09.018>

497 Godfrey, L., Sutherland, M., Boy, D., & Gomberg, N. (1991). Scaling of limb joint  
498 surface areas in anthropoid primates and other mammals. *Journal of*  
499 *Zoology*, 223, 603-625. [https://doi.org/10.1016/0047-2484\(89\)90067-5](https://doi.org/10.1016/0047-2484(89)90067-5)

500 Hopkins, W. D., Wesley, M. J., Izard, M. K., Hook, M., & Schapiro, S. J. (2004).  
501 Chimpanzees (*Pan troglodytes*) are predominantly right-handed: replication  
502 in three populations of apes. *Behavioral Neuroscience*, 118, 659.  
503 <https://doi.org/10.1037/0735-7044.118.3.659>

504 Howell, S. M., & Galinat, B. J. (1989). The glenoid–labral socket: A constrained  
505 articular surface. *Clinical Orthopaedics and Related Research*, 243, 122-  
506 125. <https://doi.org/10.1097/00003086-198906000-00018>

507 Hunt, K. D. (1991). Positional behavior in the Hominoidea. *International Journal*  
508 *of Primatology*, 12, 95-118. <https://doi.org/10.1007/BF02547576>

509 Isler, K. (2005). 3D-kinematics of vertical climbing in hominoids. *American*  
510 *Journal of Physical Anthropology*, 126, 66-81.  
511 <https://doi.org/10.1002/ajpa.10419>

512 Jungers, W. L. (1991). Scaling of postcranial joint size in hominoid primates.  
513 *Human Evolution*, 6, 391-399. <https://doi.org/10.1007/BF02435532>

514 Katz, D., & Friess, M. (2014). 3D from standard digital photography of human  
515 crania—a preliminary assessment. *American Journal of Physical*  
516 *Anthropology*, 154, 152-158. <https://doi.org/10.1002/ajpa.22468>

517 Klingenberg, C. P. (2011). MorphoJ: an integrated software package for geometric  
518 morphometrics. *Molecular ecology resources*, 11, 353-357.  
519 <https://doi.org/10.1111/j.1755-0998.2010.02924.x>

520 Lague, M. R., & Jungers, W. L. (1999). Patterns of sexual dimorphism in the  
521 hominoid distal humerus. *Journal of Human Evolution*, 36, 379-399.  
522 <https://doi.org/10.1006/jhev.1998.0274>

523 Larson, S. G., & Stern Jr, J. T. (1986). EMG of scapulohumeral muscles in the  
524 chimpanzee during reaching and “arboreal” locomotion. *American Journal*  
525 *of Anatomy*, 176, 171-190. <https://doi.org/10.1002/aja.1001760207>

526 Larson, S. G. (1988). Subscapularis function in gibbons and chimpanzees:  
527 implications for interpretation of humeral head torsion in hominoids.  
528 *American Journal of Physical Anthropology*, 76, 449-462.  
529 <https://doi.org/10.1002/ajpa.1330760405>

530 Larson, S. G. (1995). New  
531 characters for the functional interpretation of primate scapulae and proximal  
532 humeri. *American Journal of Physical Anthropology*, 98, 13-35.  
533 <https://doi.org/10.1002/ajpa.1330980103>

534 Larson, S.G. (2013). Shoulder Morphology in Early Hominin Evolution. In Reed,  
535 K., Fleagle, J., Leakey, R. (Eds), *The Paleobiology of Australopithecus.*  
536 *Vertebrate Paleobiology and Paleoanthropology* (pp. 247–261). Springer.  
537 [https://doi.org/10.1007/978-94-007-5919-0\\_17](https://doi.org/10.1007/978-94-007-5919-0_17)

538 Macias, M. E., & Churchill,  
539 S. E. (2015). Functional morphology of the Neandertal scapular glenoid  
540 fossa. *The Anatomical Record*, 298, 168-179.  
541 <https://doi.org/10.1002/ar.23072>

542 MaClatchy, L., Gebo, D., Kityo, R., & Pilbeam, D. (2000). Postcranial functional  
543 morphology of *Morotopithecus bishopi*, with implications for the evolution  
544 of modern ape locomotion. *Journal of Human Evolution*, 39, 159-183.  
545 <http://doi.org/10.1006/jhev.2000.0407>

546 Margiotoudi, K., Marie, D., Claidière, N., Coulon, O., Roth, M., Nazarian, B.,

545 Lacoste, R., Hopkins, W. D., Molesti, S. & Meguerditchian, A. (2019).  
546 Handedness in monkeys reflects hemispheric specialization within the  
547 central sulcus. An in vivo MRI study in right-and left-handed olive baboons.  
548 *Cortex*, 118, 203-211. <https://doi.org/10.1016/j.cortex.2019.01.001>

549 Morino, L., Uchikoshi, M., Bercovitch, F., Hopkins, W. D., & Matsuzawa, T.  
550 (2017). Tube task hand preference in captive hylobatids. *Primates*, 58, 403-  
551 412. <https://doi.org/10.1007/s10329-017-0605-z>

552 Preuschoft, H., Hohn, B., Scherf, H., Schmidt, M., Krause, C., & Witzel, U. (2010).  
553 Functional Analysis of the Primate Shoulder. *International Journal of*  
554 *Primateology*, 31, 301–320. <https://doi.org/10.1007/s10764-010-9399-1>

555 Roberts, D. (1974). Structure and function of the primate scapula. In Jenkins, F. A.  
556 (Ed), *Primate locomotion* (pp. 171-200). Academic Press.

557 Rohlf, F. J. (2015). The tps series of software. *Hystrix*, 26, 9-12.  
558 <https://doi.org/10.4404/hystrix-26.1-11264>

559 Rose, M. D. (1989). New postcranial specimens of catarrhines from the Middle  
560 Miocene Chinji Formation, Pakistan: descriptions and a discussion of  
561 proximal humeral functional morphology in anthropoids. *Journal of Human*  
562 *Evolution*, 18, 131-162. <http://doi.org/10.1111/j.1469-7998.1991.tb04391.x>

563 Schlager, S. (2017). Morpho and Rvcg–shape analysis in R: R-packages for  
564 geometric morphometrics, shape analysis and surface manipulations.  
565 *Statistical shape and deformation analysis* (pp. 217-256). Elsevier.  
566 <https://doi.org/10.1016/B978-0-12-810493-4.00011-0>

567 Schneider, C. A., Rasband, W. S., & Eliceiri, K. W. (2012). NIH Image to ImageJ:  
568 25 years of image analysis. *Nature methods*, 9, 671-675.  
569 <https://doi.org/10.1038/nmeth.2089>



570 Selby, M. S., Lovejoy, C. O., & Byron, C. D. (2020). Odd-nosed monkey scapular  
571 morphology converges on that of arm-swinging apes. *Journal of Human*  
572 *Evolution*, 143, 102784. <https://doi.org/10.1016/j.jhevol.2020.102784>  
573 Wiley, D. F., Amenta, N., Alcantara, D. A., Ghosh, D., Kil, Y. J., Delson, E.,  
574 Harcourt-Smith, W., Rohlf, F. J., St John, K., & Hamann, B. (2005).  
575 *Evolutionary morphing* (pp. 431-438). IEEE.  
576 <https://doi.org/10.1109/VISUAL.2005.1532826>.  
577 Young, N. M. (2008). A comparison of the ontogeny of shape variation in the  
578 anthropoid scapula: functional and phylogenetic signal. *American Journal*  
579 *of Physical Anthropology*, 136, 247-264. <https://doi.org/10.1002/ajpa.20799>

580

## 581 **Figure Legends**

582 **Figure 1.** Landmark configurations (protocols) of the glenoid cavity of the scapula  
583 used in the 3D geometric morphometric analysis with *labrum* (A) and without  
584 *labrum* (B), and in the 2D geometric morphometrics analysis with *labrum* (C) and  
585 without *labrum* (D) shown in a human glenoid (in frontal view).

586

587 **Figure 2.** PC1 vs PC2 plot derived from 3D landmarks collected on glenoid  
588 cavities without *labrum* (A) and with *labrum* (B). Deformation grids represent the  
589 shape of the outline of the glenoid cavity in anterior (frontal), and side view,  
590 superior to inferior oriented. Taxon abbreviations: Hs, *Homo sapiens*; Pt, *Pan*  
591 *troglodytes*; Hl, *Hylobates lar*; Ng, *Nomascus gabriellae*; Ph, *Papio hamadryas*;  
592 Ca, *Chlorocebus aethiops*; Cal, *Cercocebus atys lunulatus*; Mo, *Miopithecus*  
593 *ogouensis*; Cas, *Cercopithecus ascanius*.

594

595 **Figure 3.** PC1 vs PC2 plot derived from 2D landmarks collected on glenoid  
596 cavities without *labrum* (A) and with *labrum* (B). Deformation grids represent the  
597 shape of the outline of the glenoid cavity in anterior (frontal), and side view,  
598 superior to inferior oriented. Taxon abbreviations: Hs, *Homo sapiens*; Pt, *Pan*  
599 *troglodytes*; Hl, *Hylobates lar*; Ng, *Nomascus gabriellae*; Ssy, *Symphalangus*  
600 *syndactylus*; Ph, *Papio hamadryas*; Mto, *Macaca tonkeana*; Msi, *Macaca silenus*;  
601 Msy, *Macaca sylvanus*; Ca, *Chlorocebus aethiops*; Cal, *Cercocebus atys lunulatus*;  
602 Mo, *Miopithecus ogouensis*; Cas, *Cercopithecus ascanius*.

603

604 **Figure 4.** Phylogenetic (phy-)PC1 vs phy-PC2 plot derived from 3D landmarks  
605 collected on glenoid cavities without *labrum* (A) and with *labrum* (B). Deformation  
606 grids represent the shape of the outline of the glenoid cavity in anterior (frontal),  
607 and side view, superior to inferior oriented. Taxon abbreviations: Hs, *Homo*  
608 *sapiens*; Pt, *Pan troglodytes*; Hl, *Hylobates lar*; Ng, *Nomascus gabriellae*; Ph,  
609 *Papio hamadryas*; Ca, *Chlorocebus aethiops*; Cal, *Cercocebus atys lunulatus*; Mo,  
610 *Miopithecus ogouensis*; Cas, *Cercopithecus ascanius*.

611

612 **Figure 5.** Phylogentic (phy-)PC1 vs phy-PC2 plot derived from 2D landmarks  
613 collected on glenoid cavities without *labrum* (A) and with *labrum* (B). Deformation  
614 grids represent the shape of the outline of the glenoid cavity in anterior (frontal),  
615 and side view, superior to inferior oriented. Taxon abbreviations: Hs, *Homo*  
616 *sapiens*; Pt, *Pan troglodytes*; Hl, *Hylobates lar*; Ng, *Nomascus gabriellae*; Ssy,  
617 *Symphalangus syndactylus*; Ph, *Papio hamadryas*; Mto, *Macaca tonkeana*; Msi,  
618 *Macaca silenus*; Msy, *Macaca sylvanus*; Ca, *Chlorocebus aethiops*; Cal,  
619 *Cercocebus atys lunulatus*; Mo, *Miopithecus ogouensis*; Cas, *Cercopithecus*

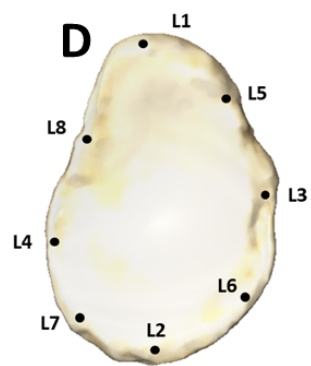
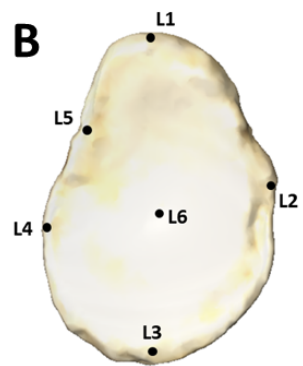
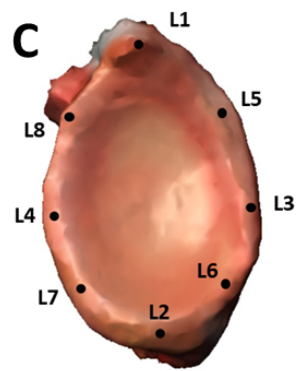
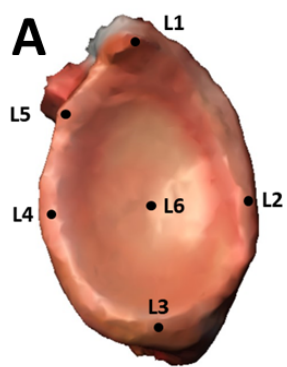
620 *ascanius*.

621

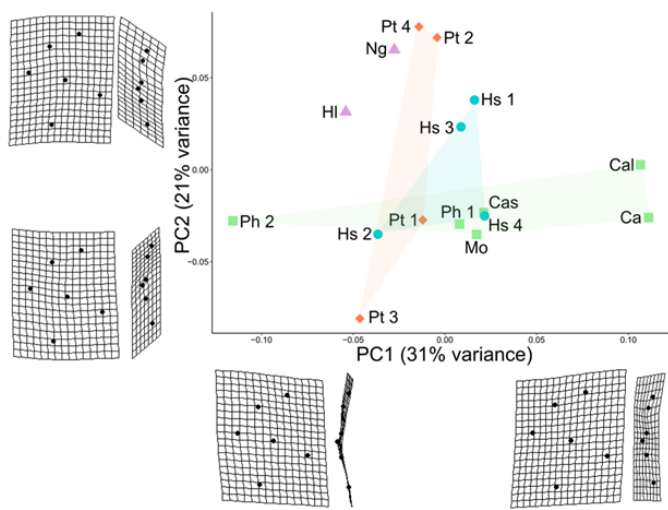
622 **Figure 6.** Box-and-whisker plot of 2D areas (cm<sup>2</sup>) of the glenoid cavity with (L)

623 and without (NoL) the glenoid labrum. Group abbreviation: Ce, cercopithecoids;

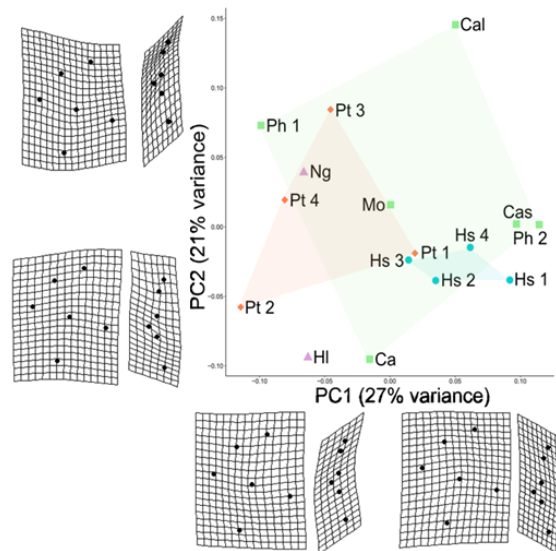
624 Hy, hylobatids; Pt, *Pan troglodytes*; Hs, *Homo sapiens*.

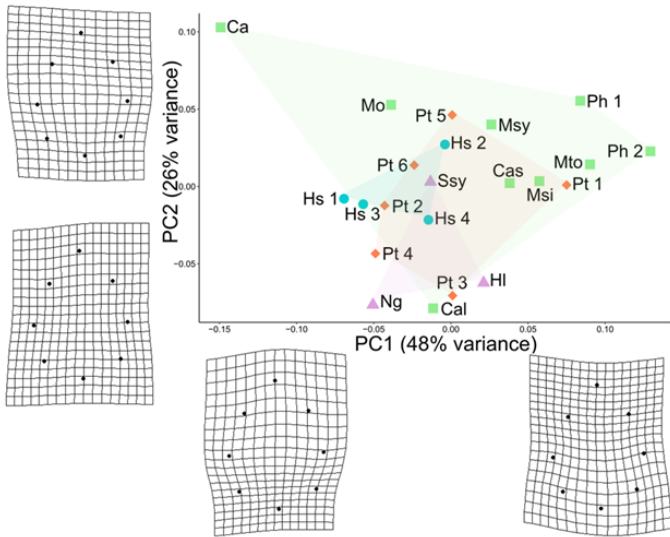
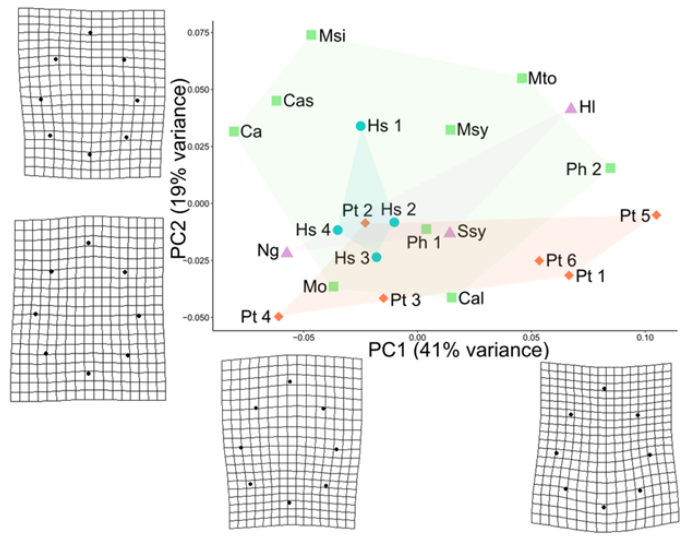


A

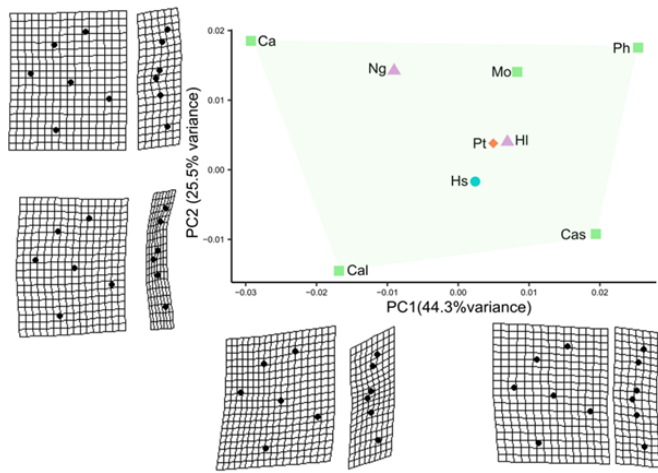


B

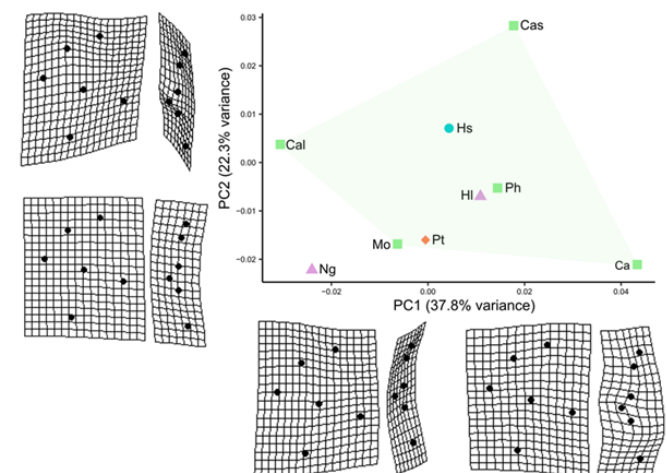


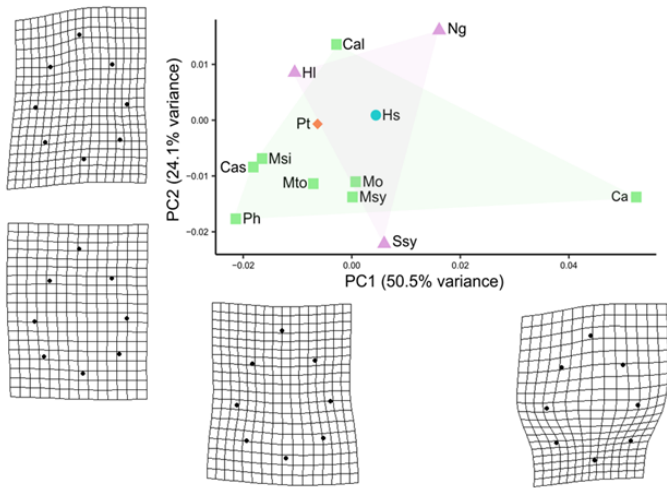
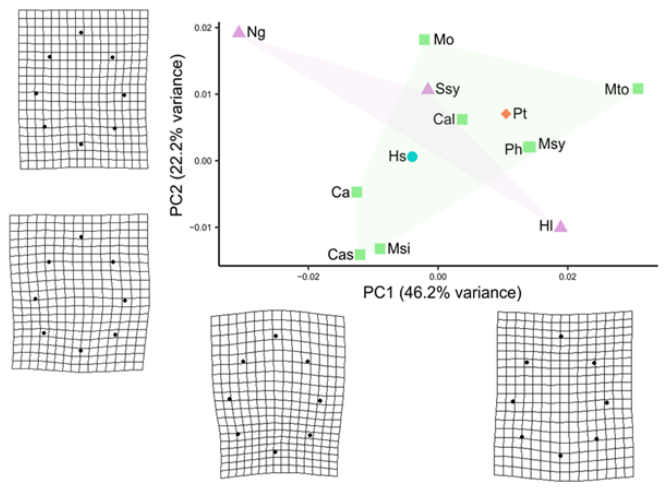
**A****B**

A



B



**A****B**



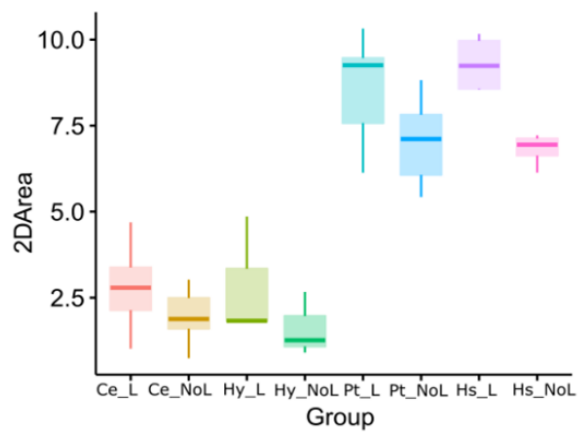


**Table 1.** Details of the comparative sample (N =22), including sample size (N), number of specimens per side (Lat), and institution.

Group	Specie	N	Lat		Institution
			R	L	
Cercopihtecines	<i>Chlorocebus aetiops</i>	1	-	1	AMUV†
	<i>Cercocebus atys lunulatus</i>	1	1	-	AMUV
	<i>Cercopithecus ascanius</i>	1	1	-	AMUV
	<i>Miopithecus ogoensis</i>	1	-	1	AMUV
	<i>Macaca silenus</i>	1	1	-	AMUV
	<i>Macaca sylvanus</i>	1	-	1	AMUV
	<i>Macaca tonkeana</i>	1	1	-	AMUV
	<i>Papio hamadryas</i>	2	1	1	AMUV
Hylobatids	<i>Symphalangus syndactylus</i>	1	1	-	AMUV
	<i>Hylobates lar</i>	1	-	1	AMUV
	<i>Nomascus gabriellae</i>	1	-	1	AMUV
<i>Pan troglodytes</i>	<i>Pan troglodytes</i>	6	3	3	AMUV
<i>Homo sapiens</i>	<i>Homo sapiens</i>	4	-	4	BDSUB†

† Abbreviations: AMUV, Anatomical Museum of the University of Valladolid; BDSUB, Body Donation Service of the Faculty of Medicine of the University of Barcelona; L, left; R, right

**Table 2.** Results for the Principal Component Analyses (PCA) with the eigenvalues (Eigenval), the variance (% Var) and the cumulative variance (% Cumul) for each Principal Component (PCs) recovered in the analyses.

PCs	3D without <i>labrum</i>			3D with <i>labrum</i>			2D without <i>labrum</i>			2D with <i>labrum</i>		
	Eigenval	% Var	% Cumul	Eigenval	% Var	% Cumul	Eigenval	% Var	Cumul %	Eigenval	% Var	% Cumul
PC1	0.00450832	36.515	36.515	0.00515790	26.840	26.840	0.00388594	48.015	48.015	0.00267182	41.403	41.403
PC2	0.00265666	21.517	58.032	0.00396391	20.627	47.467	0.00213534	26.385	74.400	0.00123629	19.158	60.560
PC3	0.00151109	12.239	70.271	0.00369729	19.240	66.707	0.00075309	9.305	83.705	0.00059673	9.247	69.807
PC4	0.00128778	10.430	80.701	0.00239042	12.439	79.146	0.00040343	4.985	88.690	0.00056658	8.780	78.587
PC5	0.00076631	6.207	86.908	0.00141054	7.340	86.486	0.00022726	2.808	91.498	0.00042669	6.612	85.199
PC6	0.00061933	5.016	91.924	0.00107009	5.568	92.054	0.00020725	2.561	94.059	0.00030463	4.721	89.920
PC7	0.00042585	3.449	95.373	0.00062008	3.227	95.281	0.00016803	2.076	96.135	0.00024634	3.817	93.737
PC8	0.00028321	2.294	97.667	0.00041075	2.137	97.418	0.00012716	1.571	97.706	0.00017496	2.711	96.448
PC9	0.00017068	1.382	99.050	0.00025413	1.322	98.741	0.00009387	1.160	98.866	0.00008566	1.327	97.776
PC10	0.00007727	0.626	99.675	0.00015032	0.782	99.523	0.00005088	0.629	99.495	0.00006774	1.050	98.825
PC11	0.00004007	0.325	100.000	0.00009168	0.477	100.000	0.00003306	0.408	99.903	0.00004590	0.711	99.537
PC12	-	-	-	-	-	-	0.00000783	0.097	100.000	0.00002990	0.463	100.000

**Table 3.** Results for the Phylogenetic Principal Component Analyses with the eigenvalues (Eigenval), the variance (% Var) and the cumulative variance (% Cumul) for each Principal Component (PCs) recovered in the analyses.

	3D without <i>labrum</i>			3D with <i>labrum</i>			2D without <i>labrum</i>			2D with <i>labrum</i>		
	Eigenval	% Val	% Cumul	Eigenval	% Val	% Cumul	Eigenval	% Val	% Cumul	Eigenval	% Val	% Cumul
PC1	0.00029892	44.280	44.280	0.00051141	37.753	37.753	0.00036085	50.502	50.502	0.00026481	46.186	46.186
PC2	0.00017242	25.542	69.822	0.00030232	22.317	60.070	0.00017239	24.126	74.628	0.00012705	22.160	68.346
PC3	0.00008624	12.775	82.598	0.00020725	15.299	75.369	0.00007686	10.757	85.385	0.00005843	10.192	78.537
PC4	0.00006231	9.231	91.829	0.00014221	10.498	85.867	0.00005455	7.634	93.019	0.00004342	7.574	86.111
PC5	0.00002306	3.416	95.245	0.00011253	8.307	94.174	0.00001825	2.555	95.574	0.00003764	6.565	92.675
PC6	0.00002022	2.996	98.241	0.00006044	4.462	98.636	0.00001634	2.286	97.860	0.00001885	3.288	95.963
PC7	0.00000960	1.422	99.663	0.00001574	1.162	99.798	0.00000924	1.293	99.154	0.00001152	2.010	97.973
PC8	0.00000228	0.337	100.000	0.00000274	0.202	100.000	0.00000323	0.452	99.605	0.00000690	1.203	99.175
PC9	-	-	-	-	-	-	0.00000155	0.217	99.822	0.00000300	0.523	99.699
PC10	-	-	-	-	-	-	0.00000083	0.116	99.938	0.00000114	0.199	99.898
PC11	-	-	-	-	-	-	0.00000044	0.061	100.000	0.00000052	0.090	99.988
PC12	-	-	-	-	-	-	0.00000000	0.000	100.000	0.00000007	0.012	100.000

**Table 4.** Results of the ordinary least-squares (OLS) regression of PC scores (PC1 and PC2) vs. log-transformed centroid size (ln CS), and phylogenetic generalized least-squares (PGLS) of species mean Procrustes coordinates (Pcoords) against the mean centroid size of each group.

	OLS											
	2D without <i>labrum</i>			2D with <i>labrum</i>			3D without <i>labrum</i>			3D with <i>labrum</i>		
	R <sup>2</sup>	Adjusted R <sup>2</sup>	p-value	R <sup>2</sup>	Adjusted R <sup>2</sup>	p-value	R <sup>2</sup>	Adjusted R <sup>2</sup>	p-value	R <sup>2</sup>	Adjusted R <sup>2</sup>	p-value
PC1	0.001	-0.049	0.885	0.029	-0.019	0.448	0.009	-0.061	0.717	0.101	0.036	0.231
PC2	0.001	-0.049	0.894	0.100	0.055	0.151	0.000	-0.071	0.943	0.002	-0.069	0.880
	PGLS											
Pcoords	0.02996	-	0.766	0.01521	-	0.923	0.134	-	0.314	0.121	-	0.352

## **Supporting Information**

### **The morphofunctional implications of glenoid *labrum* of the glenohumeral joint in hominoids**

Georgina Raventós-Izard, Josep M<sup>a</sup> Potau, Aroa Casado, Juan F Pastor, Julia Arias-Martorell

## Tables

**SI Table 1.** Details of the comparative sample (N=22), including group, specimen ID, side, number of pictures taken with and without the *labrum*, and institution. Abbreviations: AMUV, Anatomical Museum of the University of Valladolid; BDSUB, Body Donation Service of the Faculty of Medicine of the University of Barcelona; L, left; R, right.

Group	Taxon	ID	Side	N pictures w/ <i>labrum</i>	N pictures w/o <i>labrum</i>	Institution
Cercopithecines	<i>Chlorocebus aetiops</i>	CA02	L	29	40	AMUV
	<i>Cercocebus atys lunulatus</i>	CAL01	R	32	53	AMUV
	<i>Cercopithecus ascanius</i>	CAS01	R	36	49	AMUV
	<i>Miopithecus ogoensis</i>	MO01	L	20	50	AMUV
	<i>Macaca silenus</i>	MSi03	R	21	53	AMUV
	<i>Macaca sylvanus</i>	MSY01	L	17	37	AMUV
	<i>Macaca tonkeana</i>	MTO01	R	41	52	AMUV
	<i>Papio hamadryas</i>	PH01	L	32	34	AMUV
	<i>Papio hamadryas</i>	PH03	R	32	47	AMUV
Hylobatids	<i>Symphalangus syndactylus</i>	SSy01	R	29	NE †	AMUV
	<i>Hylobates lar</i>	HL01	L	34	NE †	AMUV
	<i>Nomascus gabriellae</i>	NG03	L	100	101	AMUV
Pan troglodytes	<i>P. troglodytes</i>	PT05	L	31	47	AMUV
	<i>P. troglodytes</i>	PT06	R	24	60	AMUV
	<i>P. troglodytes</i>	PT07	R	36	53	AMUV
	<i>P. troglodytes</i>	PT08	R	27	49	AMUV
	<i>P. troglodytes</i>	PT09	L	34	40	AMUV
	<i>P. troglodytes</i>	PT10	L	24	38	AMUV
Homo sapiens	<i>H. sapiens</i>	HS051	L	96	41	BDSUB
	<i>H. sapiens</i>	HS052	L	74	29	BDSUB
	<i>H. sapiens</i>	HS053	L	79	43	BDSUB
	<i>H. sapiens</i>	HS055	L	48	23	BDSUB

† Scanning done with next engine laser scanner.

**SI Table 2.** Details of the subset of the sample (N total=16) for the 3D geometric morphometric analyses, including group, species, species sample size (N), number of specimens per side, and institution. Abbreviations: AMUV, Anatomical Museum of the University of Valladolid; BDSUB, Body Donation Service of the Faculty of Medicine of the University of Barcelona; L, left; R, right.

Group	Species	N	Side		Institution
			R	L	
Cercopithecines	<i>Chlorocebus aetiops</i>	1	-	1	AMUV
	<i>Cercocebus atys lunulatus</i>	1	1	-	AMUV
	<i>Cercopithecus ascanius</i>	1	1	-	AMUV
	<i>Miopithecus ogoensis</i>	1	-	1	AMUV
	<i>Papio hamadryas</i>	2	1	1	AMUV
Hylobatids	<i>Hylobates lar</i>	1	-	1	AMUV
	<i>Nomascus gabriellae</i>	1	-	1	AMUV
<i>Pan troglodytes</i>	<i>P. troglodytes</i>	4	3	1	AMUV
<i>Homo sapiens</i>	<i>H. sapiens</i>	4	-	4	BDSUB



**SI Table 3.** Landmark protocols applied for the 2D geometric morphometric and for the 3D geometric morphometric analyses indicating type of landmark and landmark description.

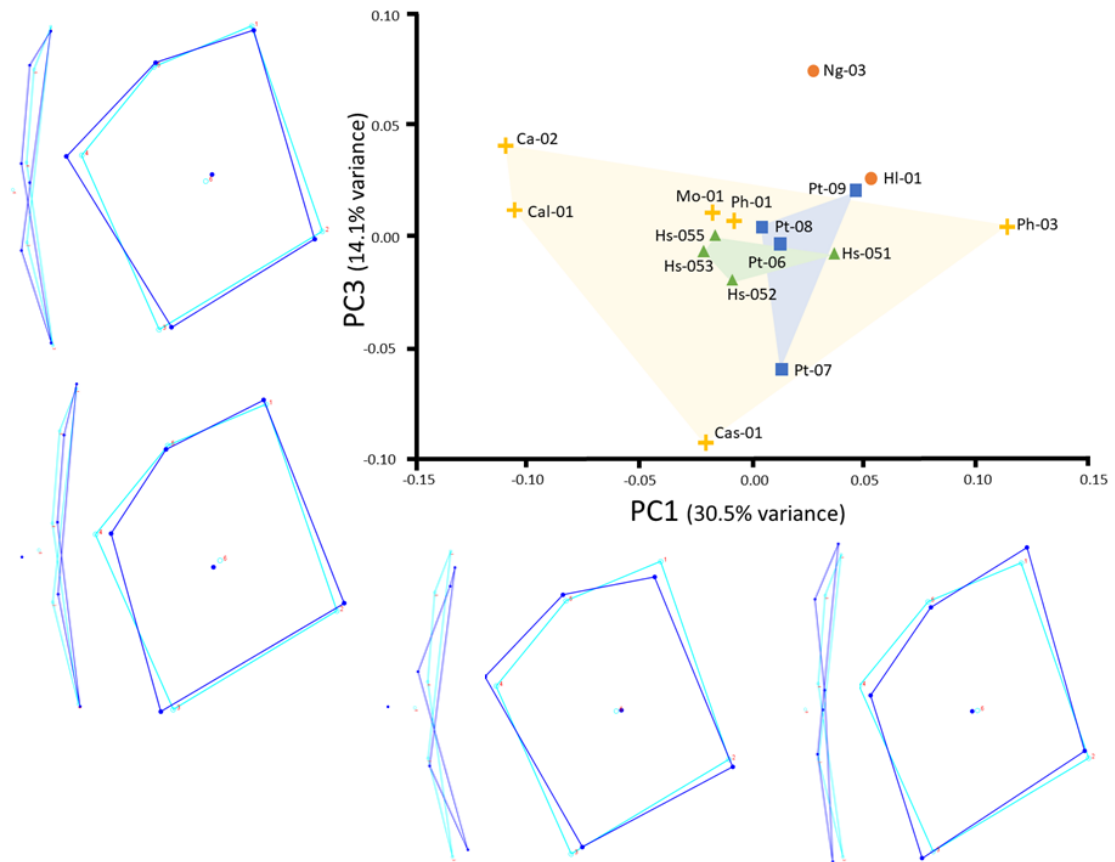
2D Landmark Protocol			3D Landmark Protocol		
Landmark	Type	Description	Landmark	Type	Description
L1	II	The most superior point of the glenoid contour	L1	II	The most superior point of the glenoid
L2	II	The most inferior point of the glenoid contour	L2	II	The most posterior point of the glenoid
L3	II	The most posterior point of the glenoid contour	L3	II	The most inferior point of the glenoid
L4	II	The most anterior point of the glenoid contour	L4	II	The most anterior point of the glenoid
L5	III	Middle point between L1 and L3	L5	III	Middle point between L1 and L4
L6	III	Middle point between L2 and L3	L6	II	Deepest point of the glenoid
L7	III	Middle point between L2 and L4	-	-	-
L8	III	Middle point between L1 and L4	-	-	-



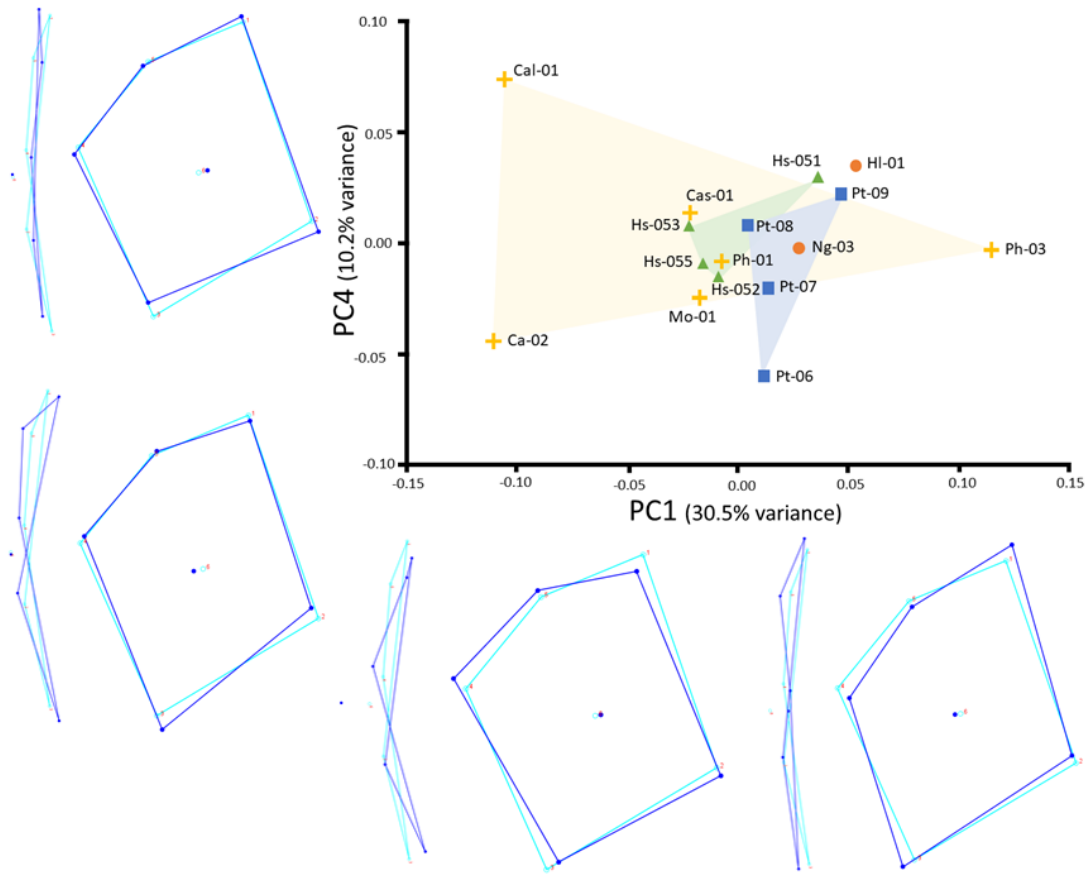
	NoL	1.000	1.000	1.000	<0.01*	1.000	0.000	1.000	1.000	0.843	1.000	1.000	1.000	1.000	0.000	0.970	1.000	1.000	<0.01*	1.000	<0.01*	1.000	1.000	1.000	1.000	1.000
--	-----	-------	-------	-------	--------	-------	-------	-------	-------	-------	-------	-------	-------	-------	-------	-------	-------	-------	--------	-------	--------	-------	-------	-------	-------	-------



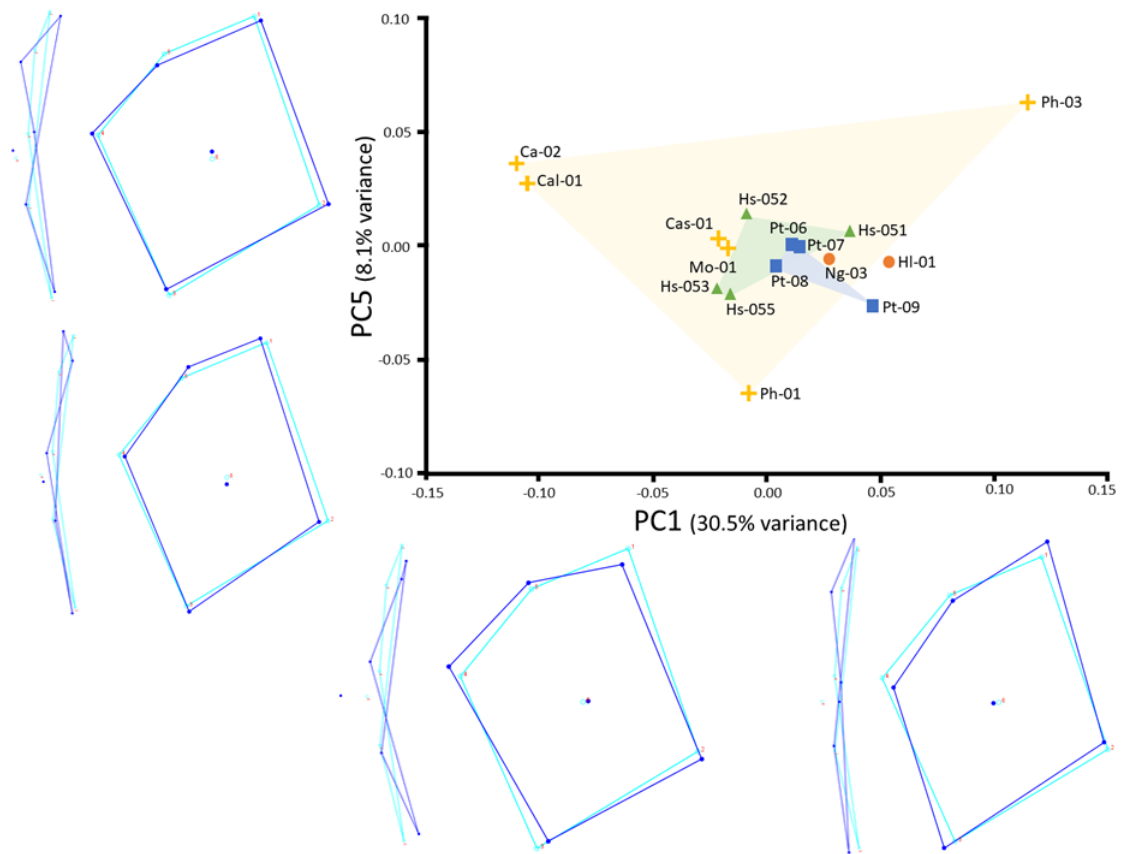
## Figures



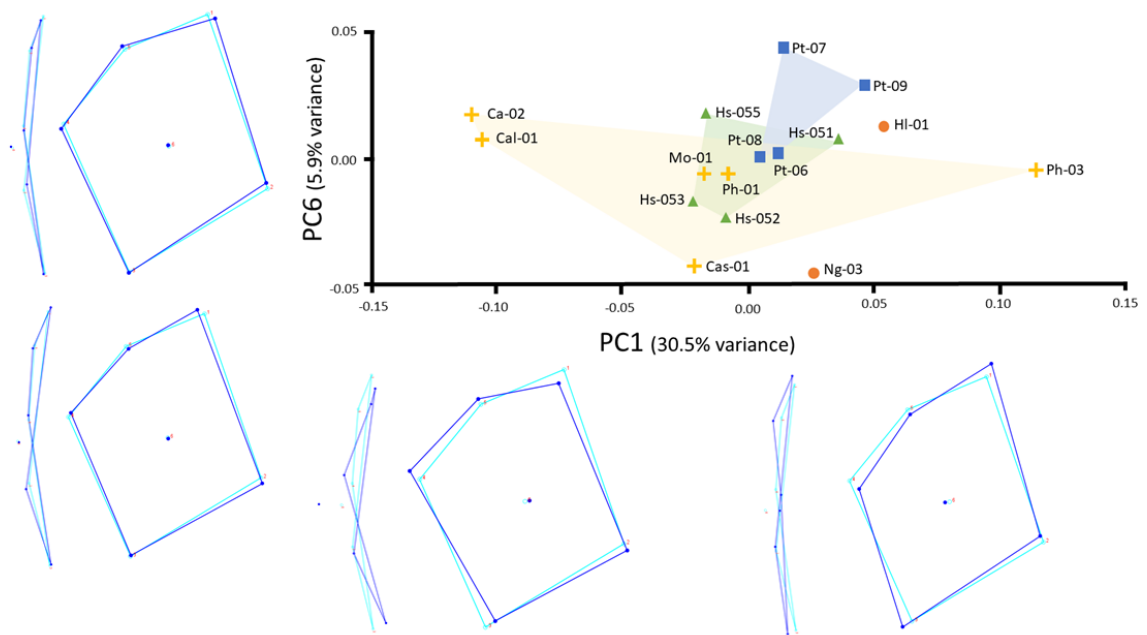
**SI Figure 1.** PC1 (30.5% of variance) vs PC3 (14.1% of variance) plot for the 3D geometric morphometric analysis of the glenoid without *labrum*. No discernible pattern or meaningful group separation was found. Wireframes represent the shape of the outline of the glenoid cavity in anterior (frontal) and side view at the end of each axis. Dark blue wireframes represent the target shape at the end of the axis and light blue wireframes represent the starting shape of the axis. Taxon abbreviations: Hs, *Homo sapiens*; Pt, *Pan troglodytes*; HI, *Hylobates lar*; Ng, *Nomascus gabriellae*; Ssy, *Symphalangus syndactylus*; Ph, *Papio hamadryas*; Mto, *Macaca tonkeana*; Msi, *Macaca silenus*; Msy, *Macaca sylvanus*; Ca, *Chlorocebus aethiops*; Cal, *Cercocebus atys lunulatus*; Mo, *Miopithecus ogouensis*; Cas, *Cercopithecus ascanius*.



**SI Figure 2.** PC1 (30.5% of variance) vs PC4 (10.2% of variance) plot for the 3D geometric morphometric analysis of the glenoid without *labrum*. No discernable pattern or meaningful group separation was found. Wireframes represent the shape of the outline of the glenoid cavity in anterior (frontal) and side view at the end of each axis. Dark blue wireframes represent the target shape at the end of the axis and light blue wireframes represent the starting shape of the axis. Taxon abbreviations: Hs, *Homo sapiens*; Pt, *Pan troglodytes*; HI, *Hylobates lar*; Ng, *Nomascus gabriellae*; Ssy, *Symphalangus syndactylus*; Ph, *Papio hamadryas*; Mto, *Macaca tonkeana*; Msi, *Macaca silenus*; Msy, *Macaca sylvanus*; Ca, *Chlorocebus aethiops*; Cal, *Cercocebus atys lunulatus*; Mo, *Miopithecus ogouensis*; Cas, *Cercopithecus ascanius*.

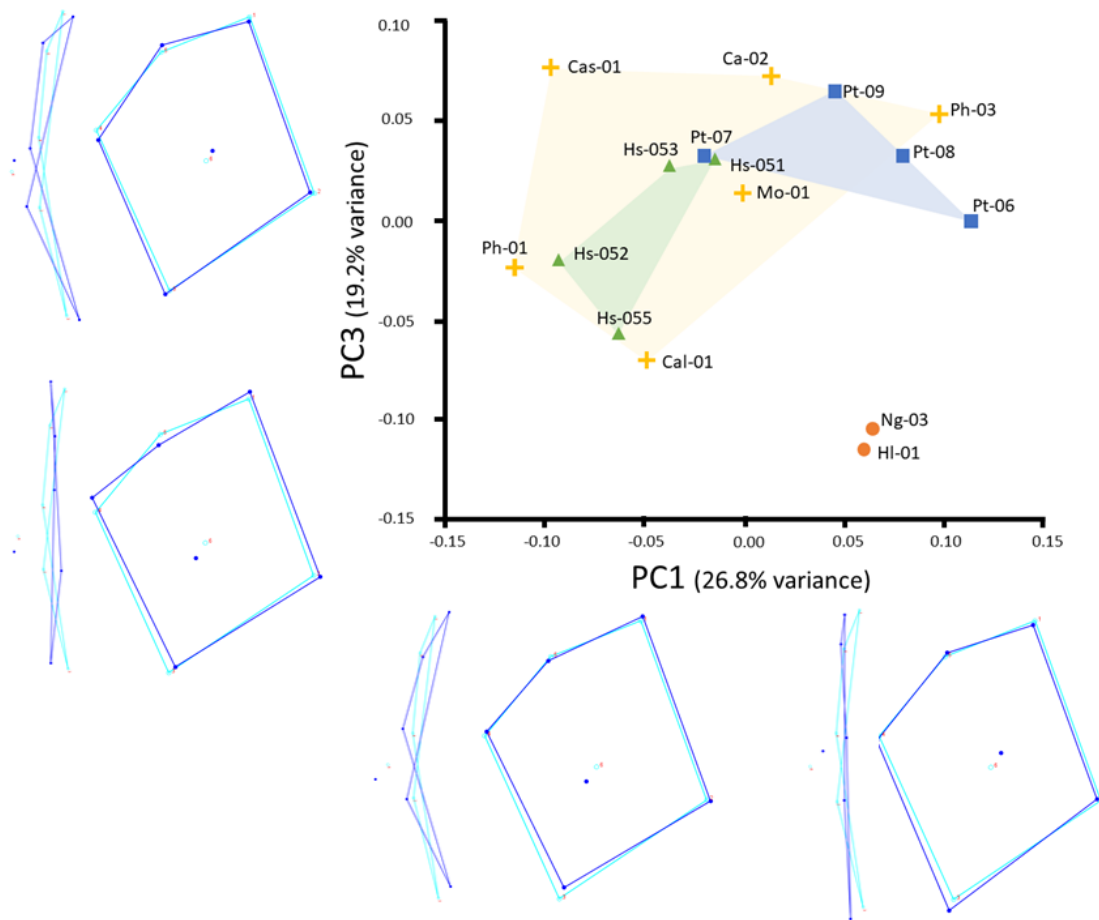


**SI Figure 3.** PC1 (30.5% of variance) vs PC5 (8.1% of variance) plot for the 3D geometric morphometric analysis of the glenoid without *labrum*. No discernable pattern or meaningful group separation was found. Wireframes represent the shape of the outline of the glenoid cavity in anterior (frontal) and side view at the end of each axis. Dark blue wireframes represent the target shape at the end of the axis and light blue wireframes represent the starting shape of the axis. Taxon abbreviations: Hs, *Homo sapiens*; Pt, *Pan troglodytes*; HI, *Hylobates lar*; Ng, *Nomascus gabriellae*; Ssy, *Symphalangus syndactylus*; Ph, *Papio hamadryas*; Mto, *Macaca tonkeana*; Msi, *Macaca silenus*; Msy, *Macaca sylvanus*; Ca, *Chlorocebus aethiops*; Cal, *Cercocebus atys lunulatus*; Mo, *Miopithecus ogouensis*; Cas, *Cercopithecus ascanius*.

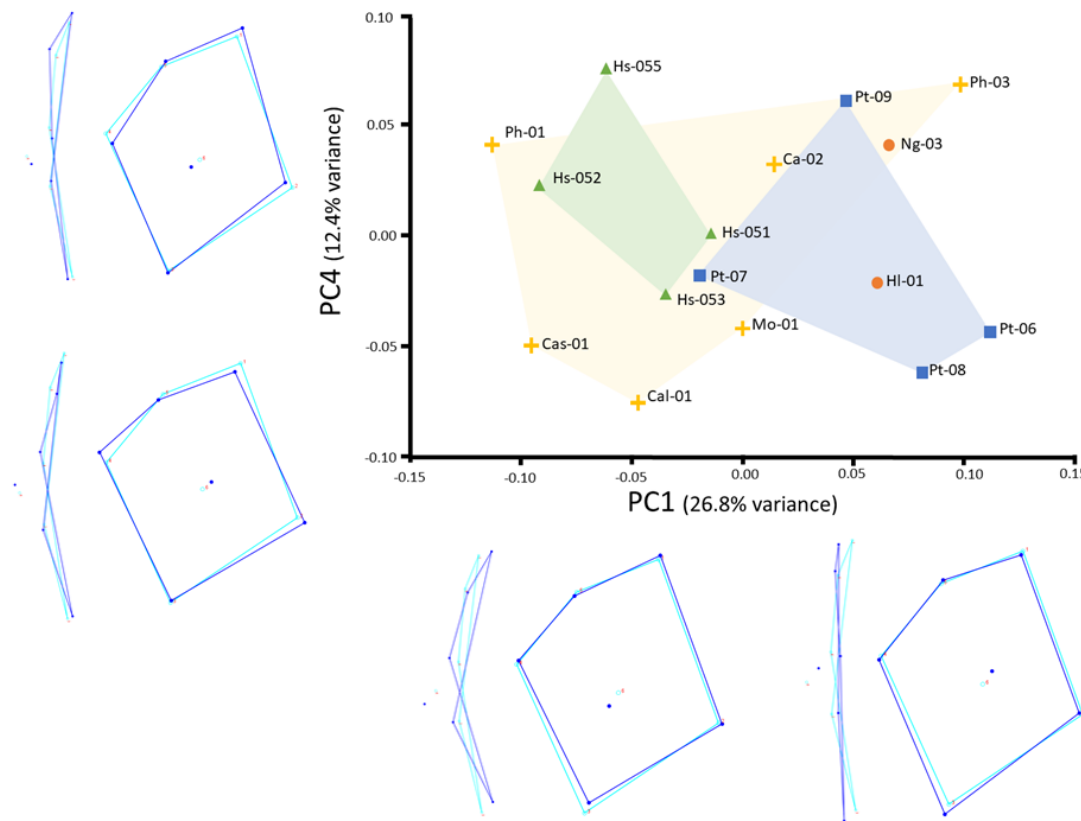


**SI Figure 4.** PC1 (30.5% of variance) vs PC6 (5.8% of variance) plot for the 3D geometric morphometric analysis of the glenoid without *labrum*. No discernable pattern or meaningful group separation was found. Wireframes represent the shape of the outline of the glenoid cavity in anterior (frontal) and side view at the end of each axis. Dark blue wireframes represent the target shape at the end of the axis and light blue wireframes represent the starting shape of the axis. Taxon abbreviations: Hs, *Homo sapiens*; Pt, *Pan troglodytes*; HI, *Hylobates lar*; Ng, *Nomascus gabriellae*; Ssy, *Symphalangus syndactylus*; Ph, *Papio hamadryas*; Mto, *Macaca tonkeana*; Msi, *Macaca silenus*; Msy, *Macaca sylvanus*; Ca, *Chlorocebus aethiops*; Cal, *Cercocebus atys lunulatus*; Mo, *Miopithecus ogouensis*; Cas, *Cercopithecus ascanius*.

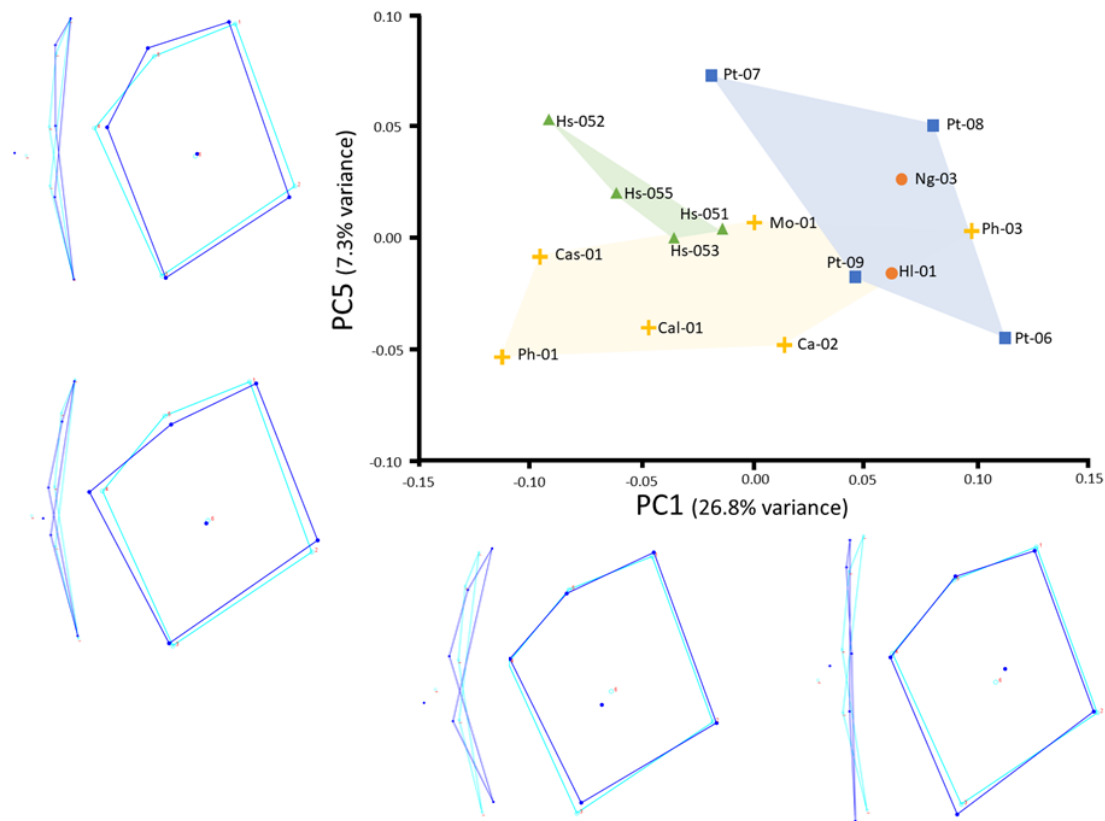




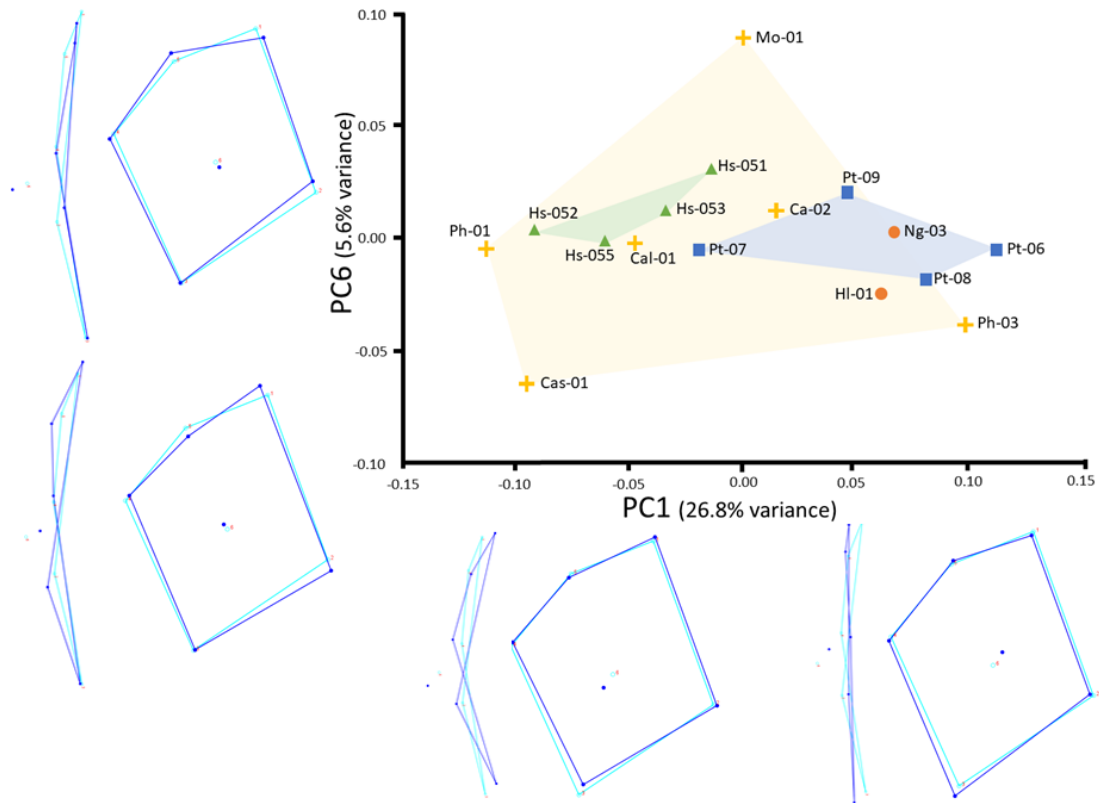
**SI Figure 5.** PC1 (26.8% of variance) vs PC3 (19.2% of variance) plot for the 3D geometric morphometric analysis of the glenoid with *labrum*. Group separation was found between hylobatids and the other groups. Wireframes represent the shape of the outline of the glenoid cavity in anterior (frontal) and side view at the end of each axis. Dark blue wireframes represent the target shape at the end of the axis and light blue wireframes represent the starting shape of the axis. Taxon abbreviations: Hs, *Homo sapiens*; Pt, *Pan troglodytes*; Hl, *Hylobates lar*; Ng, *Nomascus gabriellae*; Ssy, *Symphalangus syndactylus*; Ph, *Papio hamadryas*; Mto, *Macaca tonkeana*; Msi, *Macaca silenus*; Msy, *Macaca sylvanus*; Ca, *Chlorocebus aethiops*; Cal, *Cercocebus atys lunulatus*; Mo, *Miopithecus ouguensis*; Cas, *Cercopithecus ascanius*.



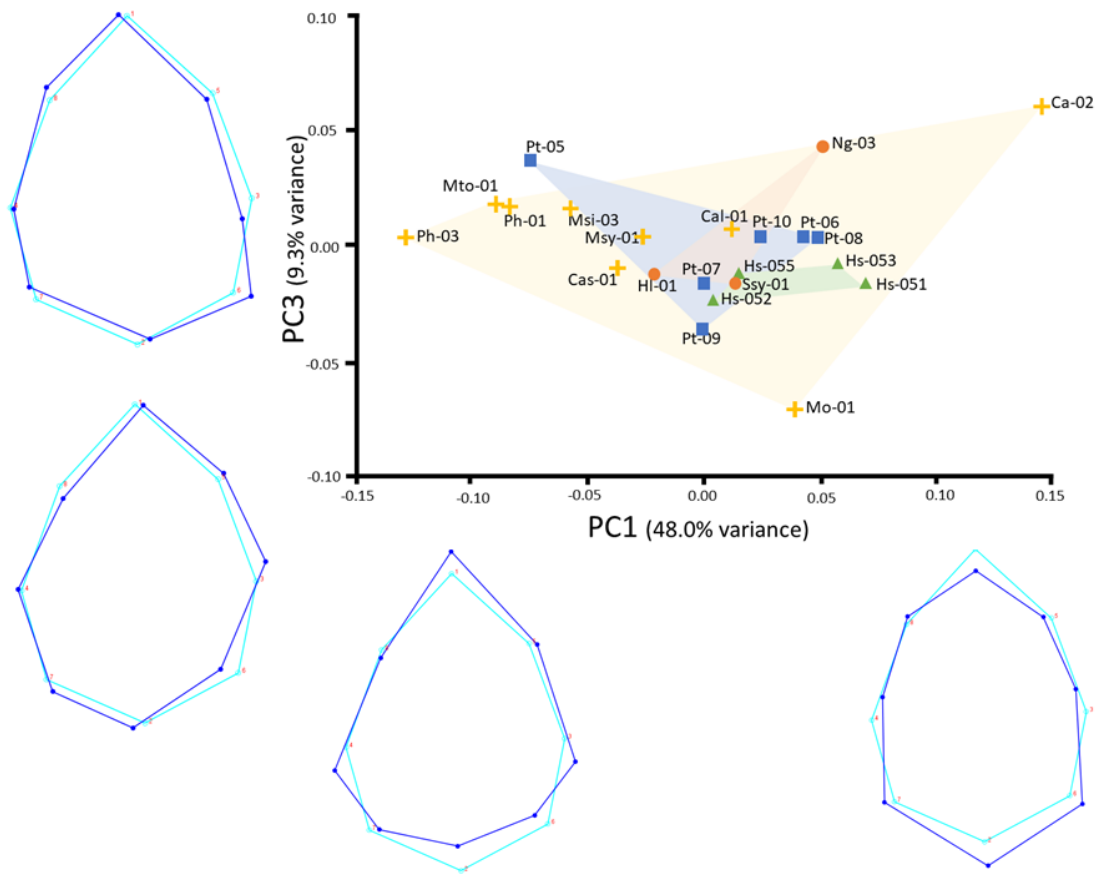
**SI Figure 6.** PC1 (26.8% of variance) vs PC4 (12.4% of variance) plot for the 3D geometric morphometric analysis of the glenoid with *labrum*. No discernable pattern or meaningful group separation was found. Wireframes represent the shape of the outline of the glenoid cavity in anterior (frontal) and side view at the end of each axis. Dark blue wireframes represent the target shape at the end of the axis and light blue wireframes represent the starting shape of the axis. Taxon abbreviations: Hs, *Homo sapiens*; Pt, *Pan troglodytes*; HI, *Hylobates lar*; Ng, *Nomascus gabriellae*; Ssy, *Symphalangus syndactylus*; Ph, *Papio hamadryas*; Mto, *Macaca tonkeana*; Msi, *Macaca silenus*; Msy, *Macaca sylvanus*; Ca, *Chlorocebus aethiops*; Cal, *Cercocebus atys lunulatus*; Mo, *Miopithecus ogouensis*; Cas, *Cercopithecus ascanius*.



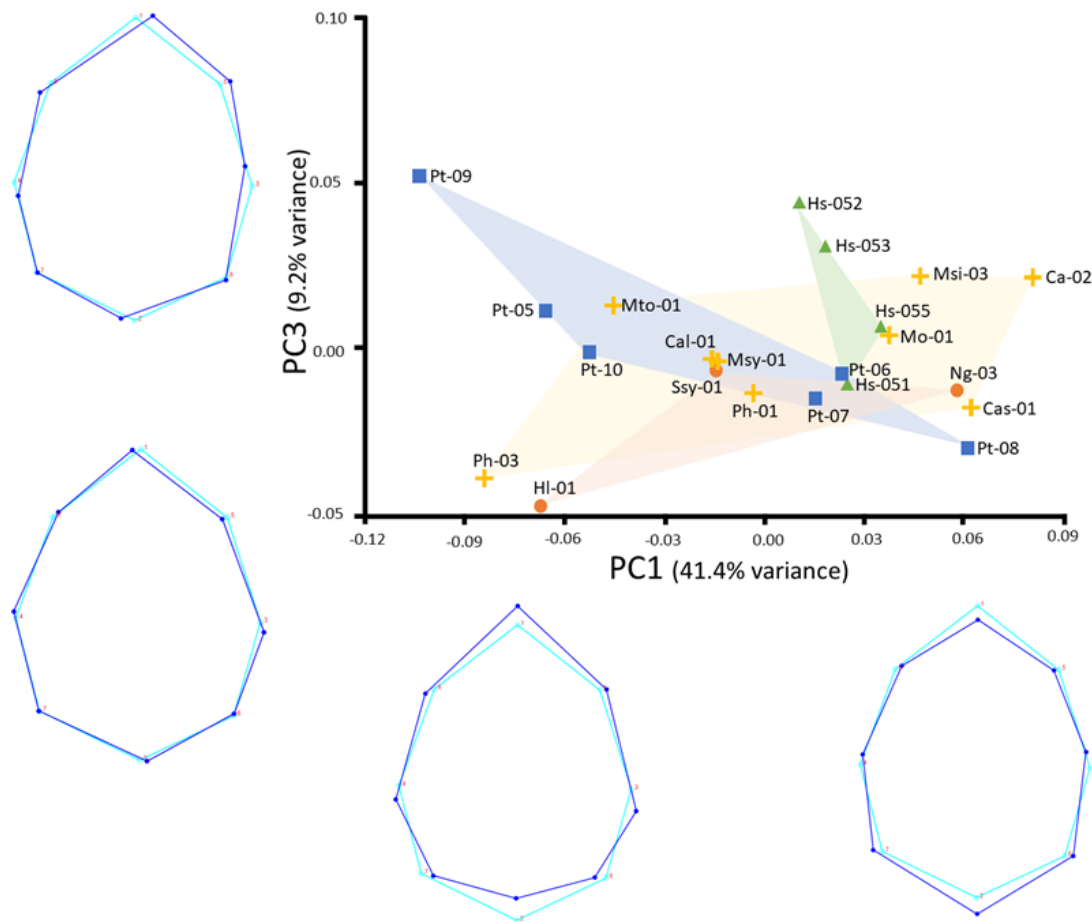
**SI Figure 7.** PC1 (26.8% of variance) vs PC5 (7.3 % of variance) plot for the 3D geometric morphometric analysis of the glenoid with *labrum*. No discernable pattern or meaningful group separation was found. Wireframes represent the shape of the outline of the glenoid cavity in anterior (frontal) and side view at the end of each axis. Dark blue wireframes represent the target shape at the end of the axis and light blue wireframes represent the starting shape of the axis. Taxon abbreviations: Hs, *Homo sapiens*; Pt, *Pan troglodytes*; HI, *Hylobates lar*; Ng, *Nomascus gabriellae*; Ssy, *Symphalangus syndactylus*; Ph, *Papio hamadryas*; Mto, *Macaca tonkeana*; Msi, *Macaca silenus*; Msy, *Macaca sylvanus*; Ca, *Chlorocebus aethiops*; Cal, *Cercocebus atys lunulatus*; Mo, *Miopithecus ogouensis*; Cas, *Cercopithecus ascanius*.



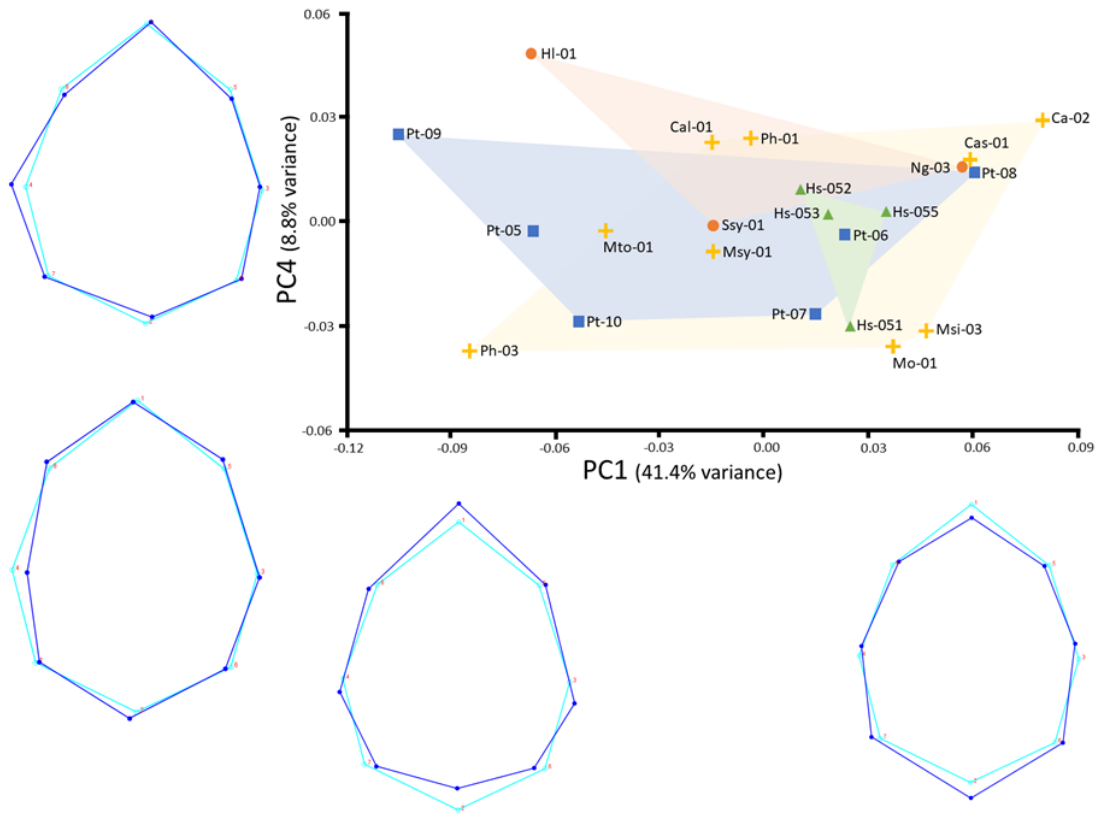
**SI Figure 8.** PC1 (26.8% of variance) vs PC6 (5.5% of variance) plot for the 3D geometric morphometric analysis of the glenoid with *labrum*. No discernable pattern or meaningful group separation was found. Wireframes represent the shape of the outline of the glenoid cavity in anterior (frontal) and side view at the end of each axis. Dark blue wireframes represent the target shape at the end of the axis and light blue wireframes represent the starting shape of the axis. Taxon abbreviations: Hs, *Homo sapiens*; Pt, *Pan troglodytes*; HI, *Hylobates lar*; Ng, *Nomascus gabriellae*; Ssy, *Symphalangus syndactylus*; Ph, *Papio hamadryas*; Mto, *Macaca tonkeana*; Msi, *Macaca silenus*; Msy, *Macaca sylvanus*; Ca, *Chlorocebus aethiops*; Cal, *Cercocebus atys lunulatus*; Mo, *Miopithecus ogouensis*; Cas, *Cercopithecus ascanius*.



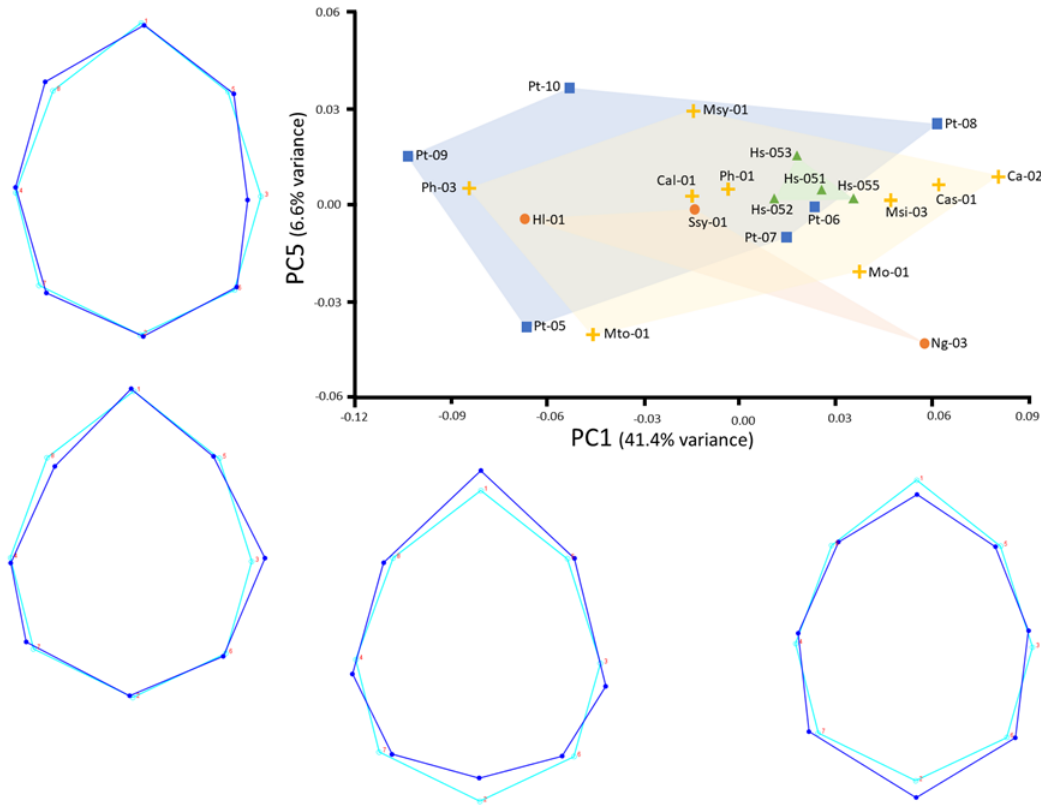
**SI Figure 9.** PC1 (48.0% of variance) vs PC3 (9.3% variance) plot for the 2D geometric morphometric analysis of the glenoid without *labrum*. No discernable pattern or meaningful group separation was found. Wireframes represent the shape of the outline of the glenoid cavity in anterior (frontal) view at the end of each axis. Dark blue wireframes represent the target shape at the end of the axis and light blue wireframes represent the starting shape of the axis. Taxon abbreviations: Hs, *Homo sapiens*; Pt, *Pan troglodytes*; HI, *Hylobates lar*; Ng, *Nomascus gabriellae*; Ssy, *Symphalangus syndactylus*; Ph, *Papio hamadryas*; Mto, *Macaca tonkeana*; Msi, *Macaca silenus*; Msy, *Macaca sylvanus*; Ca, *Chlorocebus aethiops*; Cal, *Cercocebus atys lunulatus*; Mo, *Miopithecus ogouensis*; Cas, *Cercopithecus ascanius*.



**SI Figure 10.** PC1 (41.4% of variance) vs PC3 (9.2% of variance) plot for the 2D geometric morphometric analysis of the glenoid with *labrum*. No discernable pattern or meaningful group separation was found. Wireframes represent the shape of the outline of the glenoid cavity in anterior (frontal) view at the end of each axis. Dark blue wireframes represent the target shape at the end of the axis and light blue wireframes represent the starting shape of the axis. Taxon abbreviations: Hs, *Homo sapiens*; Pt, *Pan troglodytes*; Hl, *Hylobates lar*; Ng, *Nomascus gabriellae*; Ssy, *Symphalangus syndactylus*; Ph, *Papio hamadryas*; Mto, *Macaca tonkeana*; Msi, *Macaca silenus*; Msy, *Macaca sylvanus*; Ca, *Chlorocebus aethiops*; Cal, *Cercocebus atys lunulatus*; Mo, *Miopithecus ogouensis*; Cas, *Cercopithecus ascanius*.



**SI Figure 11.** PC1 (41.4% of variance) vs PC4 (8.8% of variance) plot for the 2D geometric morphometric analysis of the glenoid with *labrum*. No discernable pattern or meaningful group separation was found. Wireframes represent the shape of the outline of the glenoid cavity in anterior (frontal) view at the end of each axis. Dark blue wireframes represent the target shape at the end of the axis and light blue wireframes represent the starting shape of the axis. Taxon abbreviations: Hs, *Homo sapiens*; Pt, *Pan troglodytes*; Hl, *Hylobates lar*; Ng, *Nomascus gabriellae*; Ssy, *Symphalangus syndactylus*; Ph, *Papio hamadryas*; Mto, *Macaca tonkeana*; Msi, *Macaca silenus*; Msy, *Macaca sylvanus*; Ca, *Chlorocebus aethiops*; Cal, *Cercocebus atys lunulatus*; Mo, *Miopithecus ogouensis*; Cas, *Cercopithecus ascanius*.



**SI Figure 12.** PC1 (41.4% of variance) vs PC5 (6.6% of variance) plot for the 2D geometric morphometric analysis of the glenoid with *labrum*. No discernable pattern or meaningful group separation was found. Wireframes represent the shape of the outline of the glenoid cavity in anterior (frontal) view at the end of each axis. Dark blue wireframes represent the target shape at the end of the axis and light blue wireframes represent the starting shape of the axis. Taxon abbreviations: Hs, *Homo sapiens*; Pt, *Pan troglodytes*; HI, *Hylobates lar*; Ng, *Nomascus gabriellae*; Ssy, *Symphalangus syndactylus*; Ph, *Papio hamadryas*; Mto, *Macaca tonkeana*; Msi, *Macaca silenus*; Msy, *Macaca sylvanus*; Ca, *Chlorocebus aethiops*; Cal, *Cercocebus atys lunulatus*; Mo, *Miopithecus ogouensis*; Cas, *Cercopithecus ascanius*.